BOEING

☒ IR&D
☐ OTHER

DOCUMENT NO. D180-24987-1 MODEL

TITLE DOA LOCATION ACCURACY OF A MULTIBEAM ANTENNA SYSTEM

THE BOEING COMPANY
CODE IDENT. NO. 81205

THIS DOCUMENT IS:

CONTROLLED BY J. P. Braun 2-3709
ALL REVISIONS TO THIS DOCUMENT SHALL BE APPROVED BY THE ABOVE ORGANIZATION PRIOR TO RELEASE.

PREPARED UNDER ☐ CONTRACT NO.
☒ IR&D
☐ OTHER

DOCUMENT NO. D180-24987-1 MODEL

TITLE DOA LOCATION ACCURACY OF A MULTIBEAM ANTENNA SYSTEM

Accession For	
NTIS GRA&I	☐
DTIC TAB	☐
Unannounced	☐
Justification	
By	
Distribution/	
Availability Codes	
Dist	Avail and/or Special
A-1	

ORIGINAL RELEASE DATE 3/13/79

ISSUE NO. TO

LIMITATIONS

ADDITIONAL LIMITATIONS IMPOSED ON THIS DOCUMENT WILL BE FOUND ON A SEPARATE LIMITATIONS PAGE

PREPARED BY John P. Braun 1-17-79
SUPERVISED BY D. M. Fraser 1/19/79
APPROVED BY G. E. Ledbetter 1/22/79
J. C. Axtell 1/25/79

TABLE OF CONTENTS

		PAGE
	TITLE PAGE	i
	TABLE OF CONTENTS	ii
	REFERENCES	iii
	KEY WORDS	iv
	LIST OF ILLUSTRATIONS	v
1.0	SUMMARY	1
1.1	INTRODUCTION	1
1.2	TASK DESCRIPTION	1
1.3	METHOD OF SOLUTION	1
1.4	RESULTS	2
1.5	CONCLUSIONS	4
1.6	RECOMMENDATIONS	6
2.0	DETAILED DATA	7
2.1	BUTLER MATRIX ANTENNA	7
2.2	MODIFIED BUTLER MATRIX ANTENNA	7
2.3	CONTINUOUS BEAM STEERING	8
2.4	INTERFEROMETER ANTENNA SYSTEM	9
2.5	DOA ACCURACY DERIVATIONS	11
2.6	EXTERNAL NOISE IMPACT ON DOA ACCURACY (JAMMING)	16
2.7	CROSS POLARIZATION IMPACT ON DOA ACCURACY	18
3.0	APPENDIX	
3.1	CONTINUOUS BEAM STEERING ANALYSIS	51
3.2	HP-9820 PROGRAM FOR θ_{rms} APPROXIMATE	55
3.3	HP-9820 PROGRAM FOR θ_{rms} EXACT	57

REFERENCES

(a) R. C. Hansen: "Microwave Scanning Antennas", Volume III, "Array Systems", Academic Press, 1966

(b) N. M. Blachman: "The Effect of Noise on Bearings Obtained by Amplitude Comparison, pp 1007-1009", IEEE Transactions Aerospace and Electronic Systems", Volume AES-7, September 1971.

(c) Merrill I. Skolnik: "Introduction to Radar Systems", McGraw Hill, 1962

(d) S. A. Schelkunoff: "Antennas Theory and Practice", John Wiley & Sons, 1952

ACKNOWLEDGEMENT

The author expresses his thanks to John M. Michels for his helpful comments and discussion concerning that anathema of communication--noise.

KEY WORDS

Direction of arrival (DOA)

Interferometer

Butler Matrix-uniform distribution

Modified Butler Matrix-cosine distribution (MB)

Field of View (FOV)

Rotman Lens

Electronic Support Measures (ESM)

Jammer

LIST OF ILLUSTRATIONS

FIGURE NO.	TITLE	PAGE
1.4-1	Butler Matrix Antenna Schematic	20
1.4-2	Butler Radiation Pattern, Beam #1L at -7.18^{o}	21
1.4-3	Butler Radiation Pattern, Beam #2L at -22^{o}	22
1.4-4	Butler Radiation Pattern, Beam #3L at -38.68^{o}	23
1.4-5	Butler Radiation Pattern, Beam #4L at -61^{o}	24
1.4-6	Composite Butler Radiation Patterns, DOA Technique #1	25
1.4-7	Butler Patterns with Interferometer, DOA Technique #2	26
1.4-8	Sum and Difference of Beams 1L & 1R, DOA Technique #5	27
1.4-9	Sum and Difference of Beams 1L & 2L	28
1.4-10	Sum and Difference of Beams 2L & 3L	29
1.4-11	Sum and Difference of Beams 3L & 4L	30
1.4-12	Composite of Modified Butler Sum Beams	31
1.4-13	Modified Butler Patterns with Interferometer, DOA Technique #4	32
1.4-14	Continuous Beam Steering Pattern, DOA Technique #6	33
1.4-15	Continuous Beam Steering Pattern	34
1.4-16	Continuous Beam Steering Network	35
1.4-17	CBS Network DOA Response Characteristics (voltage)	36
1.4-18	CBS Network DOA Response Characteristics (dB)	37
1.4-19	CBS Network DOA Response Characteristics (dB)	38
1.4-20	CBS Network DOA REsponse Characteristics (dB)	39
1.4-21	CBS Network Block Diagram	40
1.4-22	Butler Patterns 1L & 1R, DOA Technique #1, DOA Accuracy	41
1.4-23	Butler Patterns 1L & 2L, DOA Technique #1, DOA Accuracy	42
1.4-24	Modified Butler Patterns 1L + 2L & 1L + 1R, DOA Technique #3, DOA Accuracy	43
1.4-25	Modified Butler Patterns 1L + 1R & 2L + 3L, DOA Technique #3, DOA Accuracy	44

LIST OF ILLUSTRATIONS (CONTINUED

FIGURE	TITLE	PAGE
1.4-26	Modified Butler Patterns , Beams 1L and 1R, DOA Technique #5, DOA Accuracy	45
1.4-27	DOA Accuracy Comparison, Butler and Modified Butler	46
1.4-28	DOA Accuracy Comparison, Butler, Modified Butler, & Interferometer	47
1.4-29	DOA Accuracy Versus Number of Pulses; Comparison of Computation Techniques for θ_{rms}	48
1.4-30	16 Element Modified Butler Doa Accuracy	49
1.4-31	External Noise Impact on DOA Accuracy	50

1.0 SUMMARY

1.1 Introduction

Many current ESM systems employ wide field of view antennas for detection and location of emitters. These systems can have their signal processing system overloaded when a large number of signals are detected, or can be rendered inoperative when as little as one high power jammer is in the field of view. Therefore, due to the large number of and differing types of emitters against which today's system must operate, a "spatial filter" capability is an absolute requirement. In addition, in order to handle the multitude of threats, the system must have a wide bandwidth and short revisit time capability. Because of these additional requirements, the best means for achieving spatial filtering is by using a multibeam antenna such as a Butler Matrix or Rotman Lens. A low-sidelobe, narrow beamwidth antenna can also provide improved system sensitivity due to its higher gain, and improved S/N ratio due to its rejection of interfering signals.

Therefore, given a multibeam antenna, how can we best utilize its aperture and capabilities to optimize the location accuracy and anti-jam capability of its ESM system, and what compromises in antenna performance must be accepted when using this optimum technique? This is the question we have addressed.

This study was performed as part of PBA 918, "Airborne Electronic Warfare Technology", and was done in support of the Strategic C^3/Airborne Intelligence Group.

1.2 Task Description

The purpose of this study was to analyze techniques for combining outputs from a multibeam antenna, such as a Butler Matrix or a Rotman Lens, in order to implement a direction of arrival (DOA) capability.

Emphasis was placed on determining the accuracy of several DOA techniques as a function of signal-to-noise (S/N) ratio with a common antenna aperture. The impact of cross polarization and sidelobes on DOA accuracy was also considered. Study results will assist in defining antenna types for ESM systems and their performance capabilities.

1.3 Method of Solution

An eight element linear array was chosen for the analysis since the geometry would then be compatible with either a Butler Matrix or Rotman Lens antenna. Radiation patterns for the "Butler" beams were computed and plotted using an HP 9820 calculator and plotter. Except where noted, the antenna aperture was held constant for all the analysis.

1.3 Method of Solution (Continued)

DOA techniques examined were as follows:

(1) Amplitude comparison between uniform illumination beams.

(2) Use edge elements as interferometer and beam selection for ambiguity resolution. Uniform illumination beams.

(3) Same as (1) except cosine illumination beams.

(4) Same as (2) except cosine illumination beams.

(5) Monopulse technique combining adjacent uniform illumination beams.

(6) Continuous beam steering with cosine illumination beams.

The DOA accuracy of these techniques was computed as a function of S/N ratio using the relationships described in Section 2.5. A comparison of relative DOA accuracy, using a common antenna aperture, was then made. Analysis was performed to determine the effect of (1) sidelobe level and (2) cross polarization on DOA accuracy.

1.4 Results

DOA Technique #1: The schematic for an eight element linear array interfaced with a Butler Matrix is shown in Figure 1.4-1. This array forms the basis for all the computations that follow. Radiation patterns for a $\lambda/2$ spacing between elements and a uniform distribution are shown in Figures 1.4-2 to 1.4-6. Only the left-hand beams are plotted since the right-hand beams are mirror images.

Since this technique uses uniform aperture illumination, it provides the maximum attainable gain value. At $\theta=0^{\circ}$, the beam crossover occurs at -3.9 dB relative to the peak of beam(s) 1L and 1R (Figure 1.4-6). The beam gain "roll-off" versus angle off broadside is dictated by the element factor and for the case considered is equal to 20 log ($\cos\theta$). The gain of the highest sidelobe for beam(s) 1 (Figure 1.4-2) is -13 dB relative to the beam peak. The difference between peak sidelobe and beam peak gain decreases with increasing angle off broadside until for beam(s) 4 (Figure 1.4-5), the difference is only 8.5 dB. The half power beam width (HPBW) for the uniform beam is

$\text{HPBW} = \frac{51}{4\cos\theta}$ where θ is the angle off broadside and the factor (4) is the effective aperture in wavelengths.

DOA Technique #2: If the end elements of the array are used as an interferometer, ambiguous solutions exist since the elements are 3.5 λ apart. The ambiguity can be resolved by determining which beamport provides the strongest

1.4 Results (Continued)

output signal. The interferometer phase difference versus DOA for the uniform illumination beams is plotted in Figure 1.4-7. The radiation pattern of the interferometer is the same as the element factor ($E=\cos\theta$), and since each interferometer element is only one element of the eight element array, its gain is -9 dB relative to the uniform illumination beams.

DOA Technique #3: The in-phase combination of two adjacent beamports, a Modified Butler (MB), yields a cosine illumination beam (Reference A). Combining the eight Butler beams by adjacent pairs via a 180° hybrid yields seven pairs of sum and difference patterns as shown on Figures 1.4-8 to 1.4-11. A composite of the sum beams is shown in Figure 1.4-12. In the formation of the MB beams, the cosine illumination function causes a loss in aperture efficiency of about 0.9 dB, and the peak sidelobe level is reduced to about -25 dB relative to the beam peak.

DOA Technique #4: Using the edge elements as an interferometer as before, the phase difference versus DOA for the MB cosine illumination beams is plotted in Figure 1.4-13. The radiation pattern and gain characteristics are the same as described above.

DOA Technique #5: The sum and difference patterns shown in Figures 1.4-8 to 1.4-11 illustrate a pseudo-monopulse technique for DOA determination. However, unlike a monopulse system the beams are fixed in space and cannot be moved in a continuous fashion. The peak sidelobe gain is only -3 dB relative to the gain of the difference pattern as shown in Figure 1.4-11.

DOA Technique #6: The radiation patterns for the in-phase combination of two MB cosine illumination beams in a 1:1 and 0.5:1 voltage combining ratio are shown in Figures 1.4-14 and 1.4-15. The beam shown in Figure 1.4-14 was formed by adding Butler beams 1L+1R to 1R+2R. The formation of two adjacent MB beams causes a 3 dB loss in gain as described in Section 2.2. A technique for combining these beams in order to provide a continuous beam steering (CBS) capability is shown in Figure 1.4-16. The response characteristics for the CBS network are shown in Figures 1.4-17 to 1.4-20 as a function of phase shifter position. A block diagram illustrating implementation of the network is shown in Figure 1.4-21.

DOA Accuracy: The performance accuracy of the DOA techniques described above is shown in Figures 1.4-22 to 1.4-26. A comparison of accuracy values as a function of S/N ratio and number of pulses averaged is shown in Figures 1.4-27 and 1.4-28. The S/N ratio values are referenced to an arbitrary field strength that would provide the designated S/N ratio, if the incoming signal arrived at the peak of the beam, at beamports 1L or 1R of the uniform array.

The relationships used for the θ_{rms} bearing error determination are described

1.4 Results (Continued)

in Sections 2.4 and 2.5. A comparison of computed θ_{rms} and approximate θ_{rms} is shown in Figure 1.4-29. The impact of averaging up to 100 DOA readings on θ_{rms} is also shown in Figure 1.4-29.

Since all of the θ_{rms} calculations described above are based upon a constant antenna aperture, it is of interest to determine the effect of doubling the antenna aperture length on θ_{rms}. If we double the length of our array to 16 elements, we will gain 3 dB in directivity. For comparison purposes θ_{rms} for a 16 element MB array was computed and plotted and is shown in Figure 1.4-30. The θ_{rms} versus S/N ratio values are again referenced to the 8 element Butler Array. Comparing Figure 1.4-30 with 1.4-24 at S/N = 20 dB, shows θ_{rms} (16) = 0.55^{o} and $\theta_{rms}(8) = 1.5^{o}$, an improvement factor of 2.8.

A signal/jammer scenario was examined in order to determine the relative DOA location performance of the Butler and MB. Results, described in Section 2.6 and Figure 1.4-31, indicate the Butler has a relatively narrow range of operation in a jamming environment when compared to the MB.

The impact of cross polarization on DOA accuracy was examined and is described in Section 2.7. Results indicate that the MB is more vulnerable to polarization induced errors than is the Butler. This result is due to the MB having a lower value for (k), the beam difference slope factor.

1.5 Conclusions

Six different DOA techniques were described in Section 1.3. Based on the results of this study, conclusions reached concerning these techniques were as follows:

DOA Technique #1: Examination of Figures 1.4-27 and 1.4-28 reveals that for P=1, this technique will provide the single lowest value for θ_{rms}, where at $\theta=0^{o}$, S/N = 11 dB, $\theta_{rms} \cong 1^{o}$. Since for the uniform beams the HPBW = 12.8^{o}, the beam-split ratio is ≅13:1. This configuration, which has the highest gain and the best single DOA performance, suffers from two major deficiencies. First, when a signal arrives near a null of one beam, a bearing error bias exists which is statistically independent of the number of readings taken. Second, the -13 dB sidelobe, as one would expect, makes the system highly vulnerable to a jammer, and can cause the bearing error to more than double when the field strengths of the jammer and signal are comparable at the antenna aperture.

1.5 Conclusions (Continued)

DOA Technique #2: Figure 1.4-28 shows that at angles away from broadside, the addition of an interferometer can improve an ESM system's overall DOA accuracy. However, since the interferometer lacks any spatial filter capability, its role is restricted to that of a passive (non-jamming) or low interference environment.

DOA Technique #3: The MB provides essentially uniform performance over the field of view (FOV). Figure 1.4-27 shows that if a large number of pulses can be averaged it will outperform the Butler by a wide margin. The beam split ratio can be arrived at from Figure 1.4-24, where $\theta = 7^{o}$, S/N = 17 dB, P=1, it equals 17/1.4 = 12:1.

Using the scenario described in Section 2.6, th lower sidelobe level of the MB gives it a definite advantage over the Butler in a jamming environment as shown in Figure 1.4-31. However, in a passive situation (with P = 1), the Butler provides the superior performance due to its higher gain.

As discussed in Section 2.7, signal amplitude measurement errors have about twice the impact on MB θ_{rms} as compared to the Butler θ_{rms}. This is due to the MB (k) factor being about one-half that of the Butler (k) factor. Analysis shows that if the ESM system lacks a polarization measurement capability, and the antenna lacks polarization purity, the error introduced in the voltage ratio measurement by a cross polarized signal can easily exceed the error caused by noise.

DOA Technique #4: Figure 1.4-28 shows that a significant improvement in DOA accuracy can be achieved by the addition of an interferometer. This technique would be useful in a non-jamming environment. Ambiguity resolution is more difficult (compared to DOA Technique #2) and requires signal strength measurement in two adjacent beam ports.

DOA Technique #5: Figure 1.4-27 shows that this configuration falls victim to the same bias error that plagues the Butler. Figure 1.4-26 shows that good DOA accuracy is achieved only over a narrow portion of the field of view. In addition, the high sidelobe level for the difference patterns, as shown in Figures 1.4-8 to 1.4-11 makes the system highly vulnerable to external interference. In short, this technique has little to offer.

DOA Technique #6: Continuous beam steering can be achieved by the method described herein, but the shape of the beam will vary with scan angle. DOA information could be derived from the phase shifter position but the adaptation time would preclude operation against anything but a steady state signal. The main advantage of the CBS may lie in the steering of the null, rather than the steering of the beam. Figures 1.4-19 and 1.4-20 show that a near "see-through" capability can be created when two signals have a small angular separation.

1.5 Conclusions (Continued)

The results of this study are generally applicable to a Rotman Lens Antenna, except that the beam shape, sidelobe level, and beam crossover parameters are more flexible in that design.

The θ_{rms} bearing error derived in this study constitutes only that portion of the total error that is due to noise. A total system error analysis must include error parameters such as: impedance mismatch loss; receiver amplitude imbalance; transmission line and equipment phase errors; beam forming network losses; receiver dynamic range limitations; polarization losses; and platform position accuracy.

1.6 Recommendations

The recommended configuration for a Butler Matrix type multibeam antenna system is one that uses several of the DOA techniques described above. The antenna baseline should be the MB with its cosine illumination beams that provide good anti-jam capability. Next, the CBS network should be an add-on so that emitters that are less than a beamwidth away from a cover jammer can be located. If the ESM system is to operate in a passive environment, the edge elements should be used as an interferometer for precise DOA information on short-on-time emitters.

If a Rotman Lens Antenna is used, a beam crossover of approximately 2 dB will provide nearly uniform location performance across the FOV. The aperture illumination function should provide a worse case sidelobe level of about -25 dB. A sidelobe level below -25 dB is not likely to be design effective because of the small reduction in the θ_{rms} that can be obtained in a jamming situation.

Extreme care must be taken in the design of the antenna aperture so that the beam voltage ratio response is constant with varing polarization, since polarization errors are likely to be the most severe error source that originates in the antenna system.

Because the results of this study are based entirely on theoretical values and relations, an experimental program should be performed whereby the accuracy of these results can be ascertained. The test antenna can be either a Butler Matrix or Rotman Lens Antenna, since both of these antenna types are currently used in operational ESM systems.

2.0 DETAILED DATA

2.1 Butler Matrix

Figures 1.4-1 to 1.4-6 illustrate the Butler matrix and its uniform illumination beams. A feature of the matrix is that each beam port has the full gain of the array, even if all beam ports are used simultaneously. Beam crossover occurs at -3.9 dB relative to the peak of the beam while the peak of a beam is coincident with the null of the adjacent beams.

The θ rms versus S/N calculations were referenced to an incoming signal arriving at the peak of beam 1L or 1R; the field strength of this signal being such that the output S/N ratio of a receiver connected to 1L or 1R is the designated value.

Figures 1.4-22 and 1.4-23 are dB plots of beams 1L, 1R & 1L, 2L radiation patterns. The voltage ratio between the two beams (DOA technique #1) which is used for DOA determination, is shown as the beam difference since -

$$20 \log \frac{V1R}{V1L} = 1R(dB) - 1L(dB)$$

The slope of the beam difference (k) is shown in dB/deg. Examination of Figures 1.4-22 and 1.4-23 reveal that the θ rms bearing error is minimum at the beam crossover and maximum at a beam null. This result is due to a bias error which is described in Section 2.5 and reference 8.

Since the S/N = 15 dB plot occurs at the peak of a beam ($\pm$ 7.18°), the S/N ratio at the crossover is actually 15-3.9 = 11.1 dB, due to the antenna gain characteristic. Therefore, for a signal arriving at the crossover angle, $\theta = 0^0$, and a receiver output S/N ratio of 11.1 dB, the θ rms bearing error is 1^0.

2.2 Modified Butler Matrix (MB)

The previous section described the uniform illumination beams formed at the output of a standard Butler Matrix. If we now combine a pair of adjacent beams in phase, we will create a new beam that has a cosine illumination function. This new beam (Σ) will suffer a gain loss of 0.92 dB relative to the peak of a uniform beam, and will have a first sidelobe that is -25 dB relative to the beam peak as shown in Figure 1.4-8 (using isotropic elements the first sidelobe is down -23 dB). By combining adjacent beam ports we can generate seven cosine illumination beams. Unfortunately we cannot form two adjacent cosine beams simultaneously without a gain loss.

Figures 1.4-8 to 1.4-11 show the Σ and Δ outputs for the cosine illumination beams. Figure 1.4-12 is a composite of the Σ beams (which are designated A-D). Referring to Figures 1.4-24 and 1.4-25, the θ_{rms} bearing error is plotted for the amplitude comparison technique using the Σ

2.2 Modified Butler Matrix (MB) (Continued)

patterns (DOA technique #3). In computing θ_{rms}, the gain values for the MB beams were lowered by 3 dB to account for the loss in the beam forming network shown below.

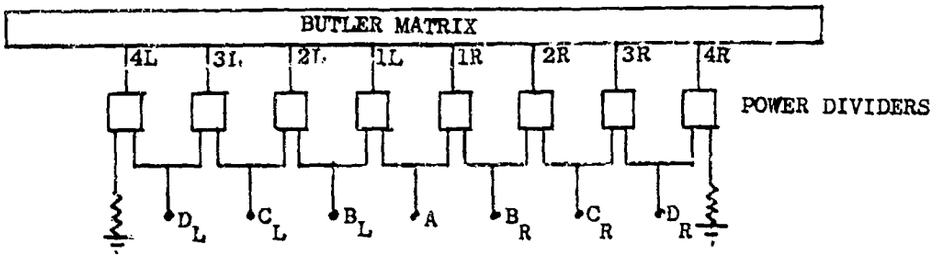

MODIFIED BUTLER (MB) OUTPUTS

For comparison purposes, if a signal arrives at the beam crossover angle of $\theta = -7.18^0$, the S/N ratio at the receiver output is 15 dB -3 -3 = 9 dB, and with P=1 then $\theta_{rms} = 2.5^0$. The poorer performance being due to the lower values for gain and the beam difference slope factor (k).

We can also use the Σ & Δ beams for our DOA determination. Note however, from Figure 1.4-8 that the sidelobes of the difference pattern are only down -10 dB relative to the peaks of the difference pattern. The θ_{rms} bearing error for amplitude comparison between Σ & Δ (DOA Technique #5) is shown in Figure 1.4-26. It can be seen that the error increases rapidly at angles beyond the crossover, which is due to a decreasing value for (k). When the DOA approaches the null, θ_{rms} increases due to the bias error described in Section 2.5.

2.3 Continuous Beam Steering (CBS)

Referring to Figure 1.4-8 and the beam complements of Figure 1.4-9, if we combine the two Σ beams, in a 1/1 amplitude ratio, we will form the beam shown in Figure 1.4-14, which has its peak near $\theta = 7^0$. If we change the combining ratio to .5/1, we have the pattern shown in Figure 1.4-15 where the beam peak is now at $\theta = 3.5^0$. It becomes apparent that by changing the amplitude combining ratio we can synthesize a new beam which can be steered between the original two beams.

A technique for implementing CBS is shown in Figure 1.4-16. The two phase shifters (ϕ_1 and ϕ_2) are ganged so that their sum is always equal to π. The derivation of the network equations, where the antenna array factor was approximated by a $\cos^n\theta$ function, is contained in Appendix 3.1. The relative signal voltage at channels A & B is plotted in Figure 1.4-17 for signal DOA's of 0^0, 7^0, and 14^0 as a function of the phase shifter position ϕ.

2.3 Continuous Beam Steering (CBS)(Continued)

Figures 1.4-18 to 1.4-20 show the relative signal level in the two channels in dB as a function of $\emptyset$. A technique for implementing the network is shown in Figure 1.4-21. If $\emptyset_1$ and $\emptyset_2$ are set to $\pi/2$, channels A and B see the original beams f_n, $f_n + 1$.

Referring to Figure 1.4-20, let us position a jammer at $\theta = 8^0$, and adjust $\emptyset$ to a value of 138^0. This maximizes the jammer signal level in channel A and minimizes it in channel B. Now if a desired emitter lies at $\theta = 7^0$ or 9^0, the S/J ratio in channel B will be enhanced by the difference between the crossover and the depth of the null. This nulling technique could provide a near see-through capability when a jammer and a desired emitter are angularly separated by less than a beam width.

The DOA of a continuous signal could also be determined by calibrating the null versus $\emptyset$ position. The accuracy of the DOA measurement would then be a function of how accurately $\emptyset$ could be measured. It is doubtful that a short-on-time pulsed emitter could be located by this technique, due to the adaptation time of the null forming loop.

2.4 Interferometer

The edge elements of the uniform array, which are 3.5 wavelengths apart, can be used as an interferometer for determining an incoming signal's DOA. The outputs from the two elements go to a pair of matched receivers and then to a phase comparator. The measured phase difference ($\emptyset$) corresponds to a family of possible angles of arrival (θn) which are determined by the following relationship.

$$\sin \theta n = \frac{\lambda}{d}\left(\frac{\phi}{2\pi} + n\right) \quad \text{where } n \text{ is an integer} \qquad (1)$$

A possible solution exists for every multiple of $\lambda/2$ spacing between elements. Referring to Figure 1.4-7, we see seven possible DOA values for any $\emptyset$. The ambiguities are resolved by measuring the relative amplitude of the signal at the Butler beam ports (DOA technique #2).

The same technique can be used with the modified Butler where the cosine beams are formed (DOA technique #4). However, referring to Figure 1.4-13, it can be seen that some of the $\emptyset$ lines nearly pass through the beam crossovers, therefore, elimination of the ambiguities is more difficult with the broader cosine beams.

If non-simultaneous operation of the interferometer and the beam forming array is satisfactory, the switching technique shown below can be used.

2.4 Interferometer (Continued)

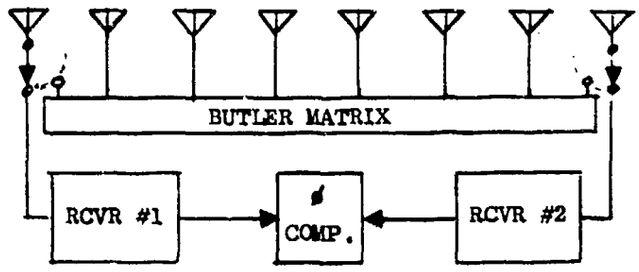

If simultaneous operation is required, some form of signal splitting technique is necessary. The technique shown below, although lossy, preserves the relative gain relations used in the analysis that follows.

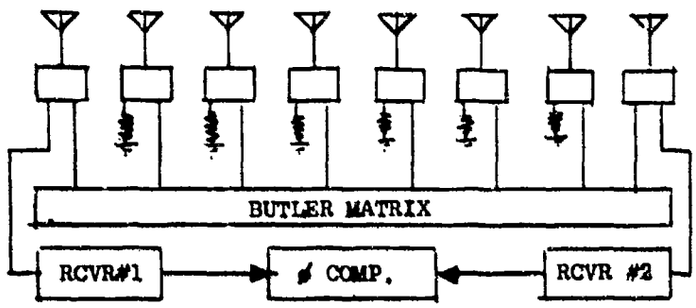

The measured phase difference $\emptyset$ is related to DOA angle θ by the relation

$$\emptyset = \frac{2\pi d}{\lambda} \sin\theta \qquad (2)$$

differentiating (2) we have

$$\frac{d\emptyset}{d\theta} = \frac{2\pi d}{\lambda} \cos\theta \qquad (3)$$

from reference (c), page 462, the error in phase measurement due to noise is -

$$\Delta\emptyset_{rms} = \left[\frac{\frac{N}{S_1} + \frac{N}{S_2}}{2P}\right]^{\frac{1}{2}} \qquad (4)$$

2.4 Interferometer (Continued)

where N/S is the noise to signal power ratio in each channel and P is the number of measurements that are averaged. Then the θ_{rms} error due to only the presence of noise is -

$$\theta_{rms} = \Delta\phi_{rms} \left(\frac{d\theta}{d\phi}\right) = \frac{\lambda \Delta\phi rms}{2\pi\, d \cos\theta} \quad \text{in radians} \qquad (5)$$

or

$$\theta^{o}_{rms} = 9.1^{o} \left(\frac{\lambda\, \Delta\phi rms}{d\ \cos\theta}\right) \quad \text{in degrees} \qquad (6)$$

Figure 1.4-28 is a plot of the interferometer θ_{rms} accuracy as compared to the Butler (uniform beams) and Modified Butler (cosine beams). In computing ϕ_{rms}, the S/N values are referenced to the peaks of beams 1L or 1R, except that the interferometer antenna gain is lower by 9 dB, which in turn lowers the S/N ratio by that value. Figure 1.4-28 is interesting in that near $\theta = 0^{o}$, the uniform beam amplitude comparison system is superior to the interferometer. This being true when noise is the only error source (in actual practice the losses in the Butler Matrix or the interferometer equipment phase errors could alter this result).

2.5 DOA Accuracy Derivation

In order to compute the DOA accuracy of a multibeam antenna amplitude comparison system, beam radiation pattern characteristics, beam difference characteristics, and the slope of the beam difference as a function of DOA must be determined. Radiation patterns were computed using the following relationships:

$$E_t = A_1 e^{j\,\psi\,1} + A_2 e^{j\,\psi\,2} + \ldots A_n e^{j\,\psi\,n} \qquad (1)$$

$$\text{where } \psi_n = \frac{2\pi\, d}{\lambda} \sin\theta + \delta \qquad (2)$$

and E_t = electric field strength

A_n = amplitude of signal in nth element

d = spacing between elements

θ = angle off broadside

δ = phase delay between elements

λ = wavelength

2.5 DOA Accuracy Derivation (Continued)

From (1), the space factor (S) as defined in reference (d) is -

$$S = \left[(A_1 \cos \psi_1 + \ldots A_n \cos \psi_n)^2 + (A_1 \sin \psi_1 + \ldots A_n \sin \psi_n)^2 \right]^{\frac{1}{2}} \quad (3)$$

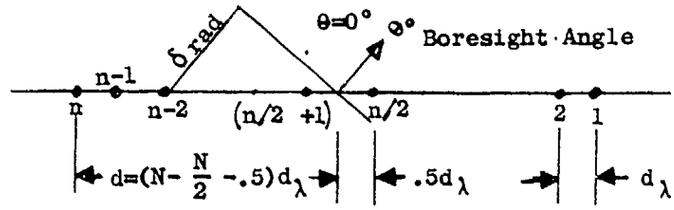

If the array is boresighted at angle θ_o, the relative phase delay for the kth element as referenced to the center of the array is δ_{rk}.

$$\delta_{rk} = 2\pi \left(k - \frac{N}{2} - 0.5\right) d_\lambda \quad \sin\theta_o \quad (4)$$

Then from (2) and (4)

$$\psi_k = 2\pi \left(k - \frac{N}{2} - 0.5\right) d_\lambda \left(\sin\theta + \sin\theta_o\right) \quad (5)$$

The impact of the element radiation patterns is introduced by multiplying the space factor (S), by the element voltage pattern. For the array described herein, a 90^0 HPBW was assumed for the element which says -

$$S' = S\cos^1\theta \quad (6)$$

The computation process then consists of defining -

N, the number of elements

d_λ , the spacing between elements in wavelengths

A_n, the element amplitude values

θ_o, the boresight angle

θ, the angle of interest

$\cos^e\theta$, the element pattern

A radiation pattern in dB is obtained by computing and plotting 10 log $(S')^2$.

2.5 DOA Accuracy Derivation (Continued)

If we have two independent patterns which are boresighted at angles θ_1 and θ_2, and we combine the two in phase, then the space factor is -

$$E_t = A_1(e^{j\psi_1} + e^{j\psi_1'}) + A_2 (e^{j\psi_2} + e^{j\psi_2'}) + \cdots A_n(e^{j\psi_n} + e^{j\psi_n'}) \quad (7)$$

which yields

$$S' = \frac{\cos^e \theta}{\sqrt{2}} \left\{ \left[\sum_1^n A_n (\cos\psi_n + \cos\psi_n')\right]^2 + \left[\sum_1^n A_n (\sin\psi_n + \sin\psi_n')\right]^2 \right\}^{\frac{1}{2}} \quad (8)$$

where $\psi = f(\theta_1)$

$\psi' = f(\theta_2)$

$\frac{1}{\sqrt{2}}$ = normalizing factor

The relationships used for computing θ_{rmsn} are taken from reference (b) and are as follows:

$$\theta_{rmsn} = \frac{8.686}{k} \sqrt{\frac{N_1 + N_2}{2P}} \quad \text{when S/N in both channels is greater than 6 dB} \quad (9)$$

where k is beam difference slope in dB/deg

N_1 and N_2 are noise-to-signal power ratios at receiver outputs.

P = the number of pulses averaged

$$\theta_{rmsn} = \frac{1}{c}\sqrt{\frac{N_{12}}{2P}} \quad \text{near a null when S/N in one channel is less than 6 dB.} \quad (10)$$

where N_{12} = ratio of noise power in null channel to signal power in sum channel

c = the beam voltage ratio slope in v/deg

$$\theta_{bias}\ \frac{1}{4c} = \sqrt{N_1\ N_{12}} \quad \text{where } -6 \text{ dB} \ll S/N \ll 6 \text{ dB} \quad (11)$$

2.5 DOA Accuracy Derivation (Continued)

$$\theta_{bias} = \frac{1}{2c}\sqrt{\pi N_{12}} \qquad \text{where S/N in null is less than -6 dB.} \qquad (12)$$

Equations (11) and (12) represent bias errors caused by noise in the null channel output. For example, in the diagram shown below if a signal arrives at θ_0, and is buried in the noise of the null channel, the ratio of the null channel output (noise) to the sum channel signal will correspond (in look-up table) to a DOA at θ_1. This then is a bias error and is independent of the number of pulses averaged.

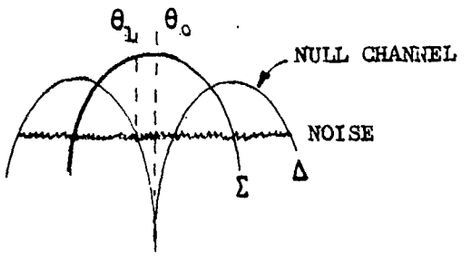

Therefore, to compute the total θ_{rms} error, we will rss the noise error of equation (10) with the bias errors of equations (11) and (12) to get -

$$\theta_{rms} = \frac{1}{c}\sqrt{N_{12}\left(\frac{1}{2P}+\frac{N_1}{16}\right)} \qquad \text{for -6 dB} < S/N < \text{6 dB} \qquad (13)$$

$$\theta_{rms} = \frac{1}{c}\sqrt{N_{12}\left(\frac{1}{2P}+\frac{\pi}{4}\right)} \qquad \text{for S/N in one channel} < \text{-6dB} \qquad (14)$$

and repeating equation (9) where no bias error exists

$$\theta_{rms} = \frac{8.686}{k}\sqrt{\frac{N_1+N_2}{2P}} \qquad \text{for S/N} > \text{6 dB in both channels} \qquad (15)$$

In the process of computing the radiation patterns, the space factor data S' (in voltage) is stored and later used to compute k and c. The noise to signal power ratios are computed by first inputting a referenced S/N ratio (in dB) at the peak of beam 1L. The antenna gain values are then used to determine the N/S power ratio existing at the angle of interest by using the following.

2.5 DOA Accuracy Derivation (Continued)

$$N_{12} = \left[10^{\frac{S/N(\text{peak in dB}) - \text{Gain Loss (dB)}}{10}} \right]^{-1} \quad (16)$$

Figure 1.4-29 is a plot of the computed θ_{rms} for the uniform illumination Butler, using equations (13), (14), and (15). Since the stepped discontinuities are unrealistic, a smoothing function was created.

From equations (10) and (12)

$$\theta_{bias} = \theta_{rmsn} \sqrt{\frac{P\pi}{2}} \quad (17)$$

then $$\theta_{rms} = \sqrt{\theta^2_{rmsn} + \frac{\theta^2_{rmsn} P \pi}{2}} \quad (18)$$

Since the last term represents the bias error, which only exists when S/N < 6 dB, we will introduce the multiplying factor (F), which is antenna gain dependent.

$$\text{let } F = \left[1 - 10^{(S/N-6+G)/10} \right]^2 \quad (19)$$

where S/N is in dB at peak of beam 1L

G is null antenna relative gain at angle of interest and is always ≤ 0.

for example, if the reference S/N = 15 dB and G=-9 (corresponding to 6 dB S/N ratio) $F = (1-10^0)^2 = 0$ and the bias term vanishes.

If the exponent is greater than 0, then the S/N ratio at the angle of interest is greater than 6 dB, so the bias term is discarded. As $G \rightarrow -\infty$, $F \rightarrow 1$, and the bias term is totally included.

Introducing the smoothing function into equation (18) we have for θ_{rms}

$$\theta_{rms} = \theta_{rmsn} \sqrt{1 + \frac{P\pi}{2} \left[1 - 10^{(S/N - 6 + G)/10} \right]^2} \quad (20)$$

θ_{rms}(approximate) is shown in Figure 1.4-29 using equation (20)

2.5 DOA Accuracy Derivation (Continued)

Doubling the length of the aperture will double the value for (k) and lower the N/S ratio by 1/2. From equation (9), the reduction factor for θ_{rms} is -

$$\frac{\frac{8.686}{k}\sqrt{\frac{N}{2}}}{\frac{8.686}{2k}\sqrt{\frac{N}{4}}} = 2\sqrt{2} = 2.8 \qquad (21)$$

The θ_{rms} calculations were performed on an HP-9820 using the programs shown in Appendices 3.2 and 3.3.

2.6 External Noise Impact on DOA Accuracy (Jamming)

If an external noise source (i.e., jammer) lies in the FOV, under certain conditions its presence can cause a significant increase in θ_{rms} bearing error. In order to determine the relative performance of the Butler and MB in a jamming environment, a scenario was examined wherein a desired signal lies at $\theta=0^{o}$, and a jamming signal eminates from $\theta=28^{o}$, where it is outside a main beam, but at the peak of a sidelobe. A minimum S/N requirement of 13 dB was chosen for signal recognition. This corresponds to a 90% probability of detection and a maximum false alarm rate of $1\ (10)^{-6}$ (Reference C, Page 34).

The analysis was performed as follows: Let's assume we have an emitter at -7.18^{o}, and its field strength is such that the S/N output of receiver 1L is 30 dB when using the Butler antenna. We will position a MB above the Butler and swing both antennas so that the emitter now lies at $\theta=0^{o}$. The S/N ratio of four identical receivers (two for each antenna) is derived from Figures 1.4-2, 1.4-6, 1.4-8 and 1.4-9. Remembering that we must lower the MB S/N ratio by an additional 3 dB due to the beamport power divider loss:

	S/N (dB)	N/S (Power)
Butler Receiver 1L	26	.0025
Butler Receiver 1R	26	.0025
MB Receiver A	26	.0025
MB Receiver B_L	17	.02

2.6 External Noise Impact on DOA Accuracy (Jamming) (Continued)

Next, let the field strength of the jammer signal when measured at our antenna, be -3 dB relative to the desired signal. Then the S/J ratios at the beamport outputs of our two antennas are:

	S/J (dB	J/S (Power)
Butler Receiver 1L	17	.02
Butler Receiver 1R	13	.05
MB Receiver A	28	.0016
MB Receiver B_L	29	.00126

Next, combining the signal, receiver noise and jammer powers:

	Total N/S (dB)	Total N/S (Power)
Butler Receiver 1L	-16	.0225
Butler Receiver 1R	-12.8	.0525
MB Receiver A	-23.8	.0041
MB Receiver B_L	-16.7	.0212

Since the S/N ratio is greater than 6 dB in all receivers, we can compute θ_{rms} using equation (9), Section 2.5.

$$\text{Butler } \theta_{rms} = \frac{8.686}{2.5}\sqrt{\frac{.0225 + .0525}{2}} = 0.673^{o} \qquad (1)$$

$$\text{MB } \theta_{rms} = \frac{8.686}{1.6}\sqrt{\frac{.0041 + .0212}{2}} = 0.612^{o} \qquad (2)$$

If we eliminate the jammer,

Butler $\theta_{rms} = 0.174^{o}$

MB $\theta_{rms} = 0.576^{o}$

The performance degradation is $\frac{.673^{o}}{.174^{o}} = 3.87$ for the Butler

2.6 External Noise Impact on DOA Accuracy (Jamming) (Continued)

and $\frac{.612^0}{.576}$ = 1.06 for the MB.

From the above, it can be seen that although the uniform illumination Butler can provide the superior performance at $\theta=0^0$, its performance is more severely affected by the presence of external noise, which is due of course to its higher sidelobe level.

The effect of S/J and S/N ratios on θ_{rms} was computed and plotted. Results are shown in Figure 1.4-31. The plot reveals that the MB can operate over a much wider S/J range, but at the sacrifice of DOA accuracy in a quiet environment.

If we compare the MB DOA accuracy with another antenna which has sidelobes that are 5 dB lower, but has the same aperture efficiency (using a Taylor Distribution),

MB receiver A---S/J = 33 dB than J/S = .0005

MB receiver B_L---S/J = 34 dB then J/S = .0004

TOTAL N/S_A = .0005 + .0025 = .003

TOTAL N/S_B = .0004 + .02 = .0204

then

$$\text{MB } \theta_{rms} = \frac{8.686}{1.6} \sqrt{\frac{.003 + .0204}{2}} = 0.587^0 \; ; \; \frac{.587}{.612} \simeq 0.96 \quad (3)$$

Therefore, lowering the peak sidelobe from -25 dB to -30 dB reduced θ_{rms} by about 4%.

2.7 Cross Polarization Impact on DOA Accuracy

If the antenna does not have a polarization measurement capability, then the output voltage ratio, which is determined by measuring an incoming signal amplitude at two adjacent beamports, will correspond to a particular DOA as determined by a "look-up table". This table will have values which are based upon the antenna's response to the calibration signal's polarization. An error may occur in the DOA determination unless the ratio is constant for all signal polarizations.

2.7 Cross Polarization Impact on DOA Accuracy (Continued)

This would require the antenna aperture to have elements which did not deviate in response with differing polarizations and angles of arrival. This characteristic may not be too difficult to obtain if the antenna is linearly polarized. However, with circular polarization an axial ratio of at least 3 dB is likely to occur somewhere in the FOV. If we assume a signal arrives at an angle where a 3 dB error occurs, a bias error will result which is a function of the beam difference slope. Referring to the beam difference line of Figure 1.4-24, if the signal arrives at -7.2°, a 3 dB error would create a bias error of $\pm 2.3^{\circ}$. With the uniform beams, the error is less pronounced due to the larger value for k and is about 1.2° near $\theta=0^{\circ}$. The total error would then be the rss of the polarization bias and the noise errors.

As can be seen from the above, the θ_{rms} error due to polarization response deficiencies can easily exceed the error due to receiver noise. If the antenna is to provide excellent DOA information for all polarizations, then it must have an excellent axial ratio or have a polarization measurement capability and corresponding look-up table.

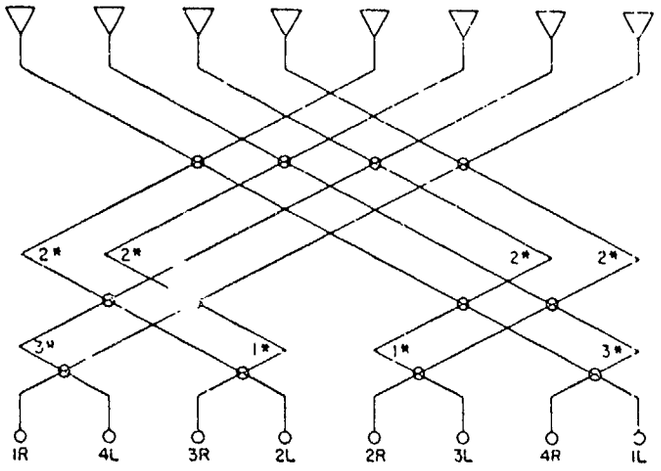

* UNITS OF PHASE SHIFT ARE π/8 RADIANS

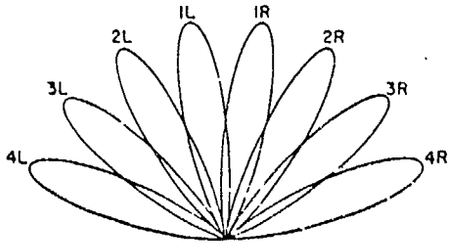

Lossless 8-element 8-beam matrix and locations of beams.

BUTLER MATRIX ANTENNA

SCHEMATIC

FIGURE 1.4-1

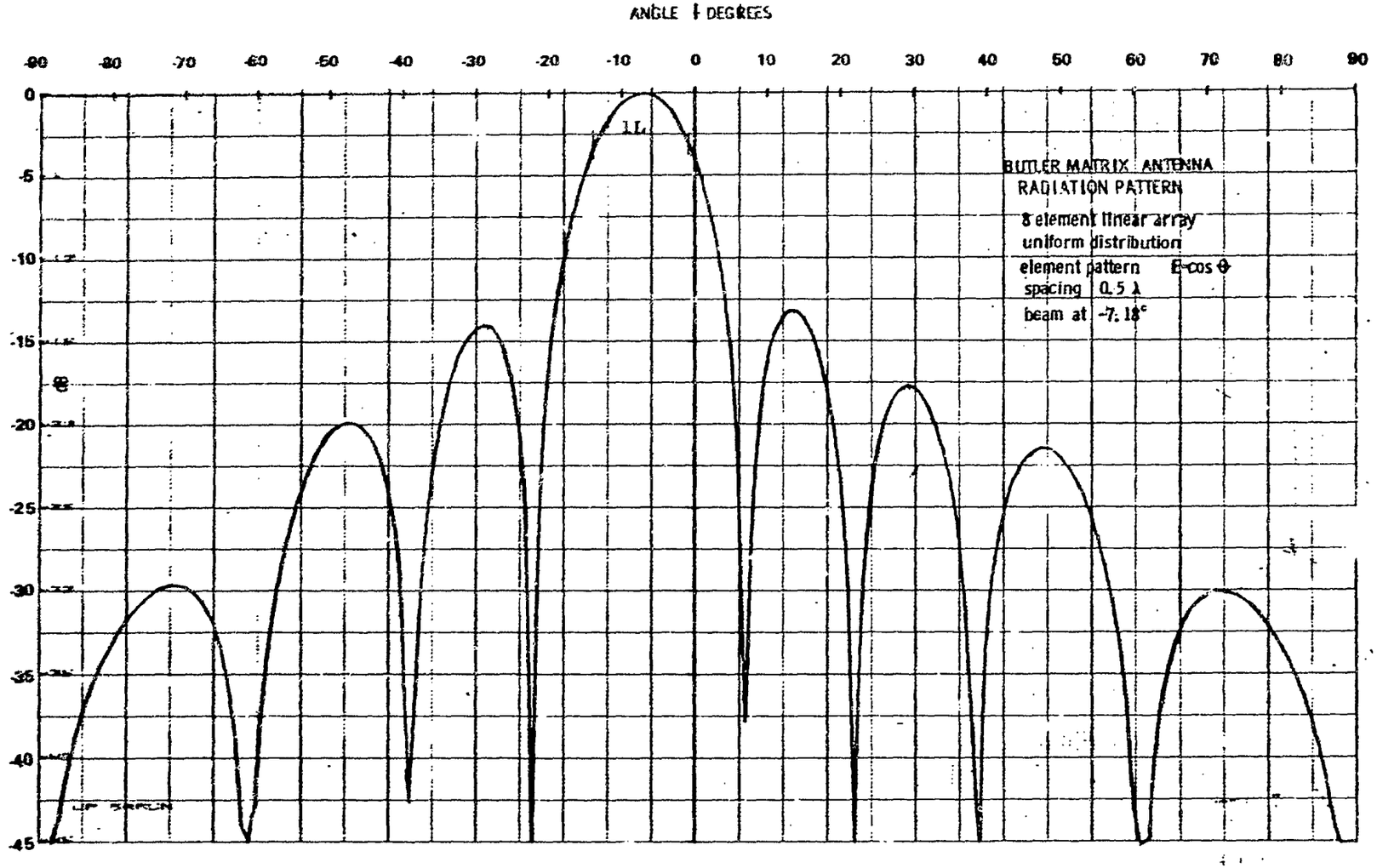
ANGLE ϕ DEGREES
-90 -80 -70 -60 -50 -40 -30 -20 -10 0 10 20 30 40 50 60 70 80 90
0 -5 -10 -15 -20 -25 -30 -35 -40 -45
dB
BUTLER MATRIX ANTENNA
RADIATION PATTERN
8 element linear array
uniform distribution
element pattern E=cos ϕ
spacing 0.5 λ
beam at -7.18°

FIGURE 1.4-2

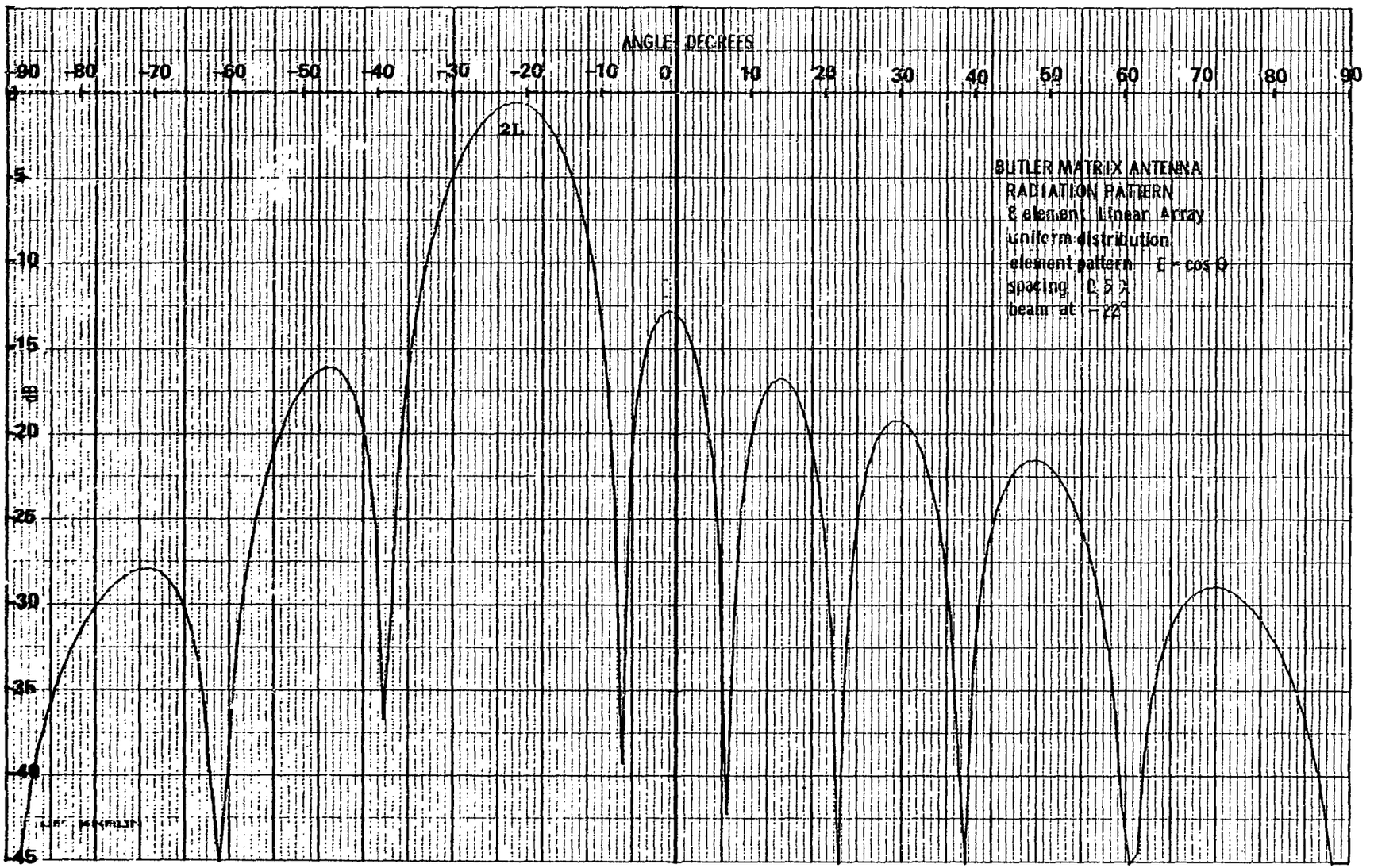
ANGLE: DECREES
-90 -80 -70 -60 -50 -40 -30 -20 -10 0 10 20 30 40 50 60 70 80 90
0
-5
-10
-15
-20
-25
-30
-35
-40
-45
dB
2L
BUTLER MATRIX ANTENNA
RADIATION PATTERN
8 element Linear Array
uniform distribution
element pattern f = cos θ
spacing 0.5 λ
beam at −22°

FIGURE 1.4-3

BUTLER MATRIX ANTENNA
RADIATION PATTERN
8 element linear array
Uniform distribution
element pattern E=cos θ
spacing 0.5 λ
beam at -38.68°
ANGLE DEGREES
-90 -80 -70 -60 -50 -40 -30 -20 -10 0 10 20 30 40 50 60 70 80 90
-5 -10 -15 -20 -25 -30 -35 -40
dB
3L

FIGURE 1.4-4

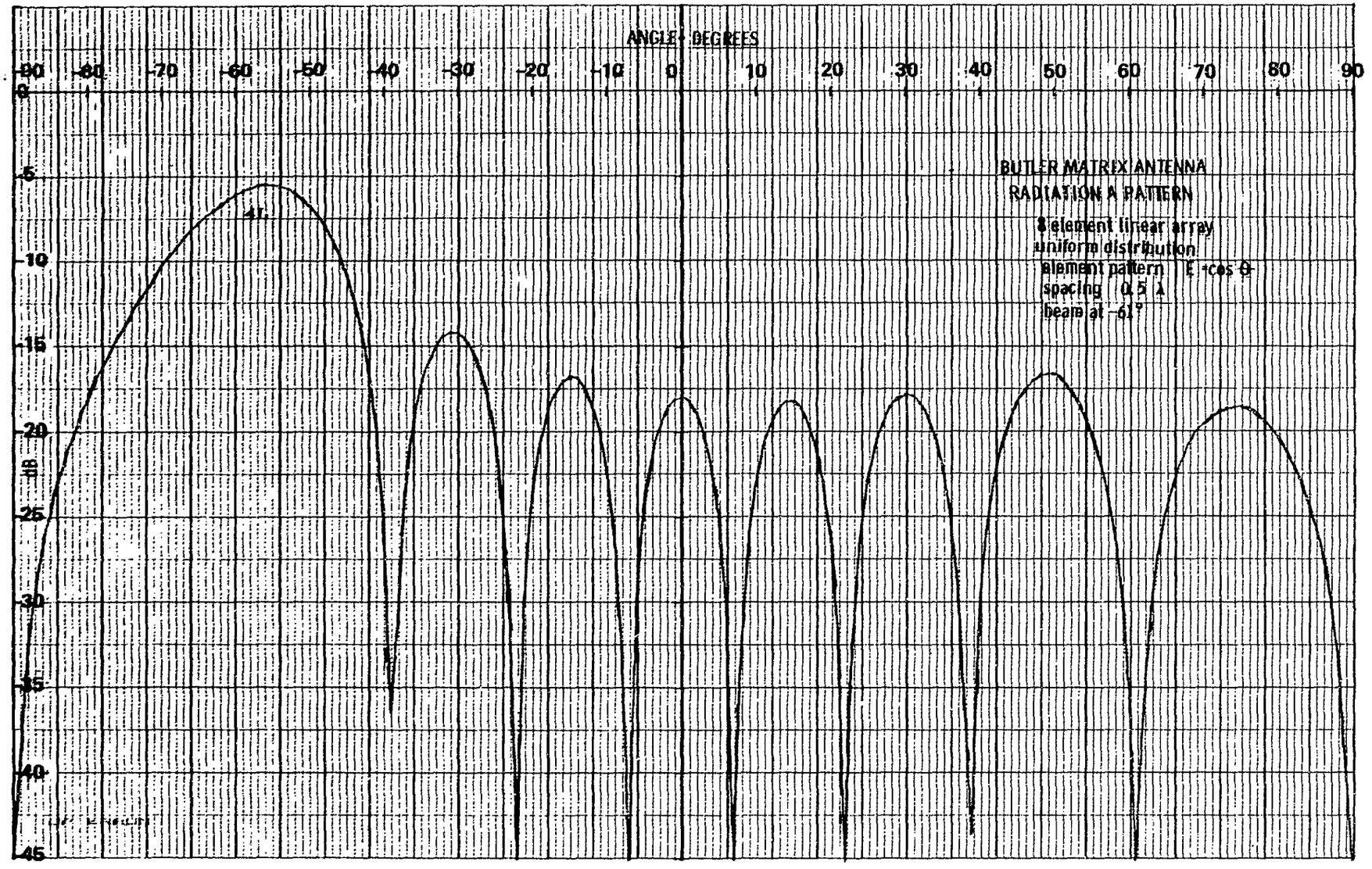
ANGLE - DEGREES
-90 -80 -70 -60 -50 -40 -30 -20 -10 0 10 20 30 40 50 60 70 80 90
0
-5
-10
-15
-20
-25
-30
-35
-40
-45
dB
-41.
BUTLER MATRIX ANTENNA
RADIATION A PATTERN
8 element linear array
uniform distribution
element pattern E ∝ cos θ
spacing 0.5 λ
beam at -61°

FIGURE 1.4-5

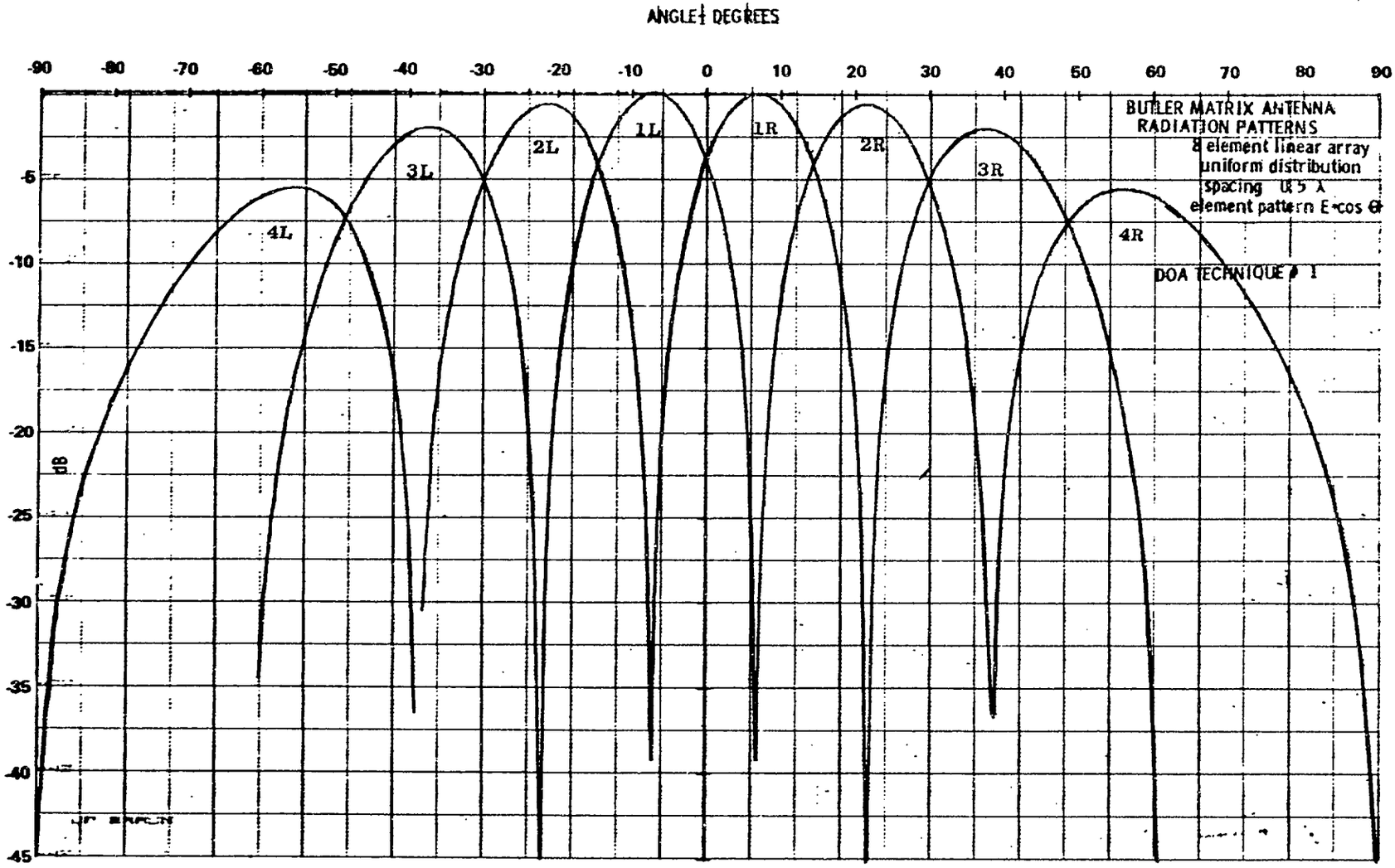
ANGLE± DEGREES
-90 -80 -70 -60 -50 -40 -30 -20 -10 0 10 20 30 40 50 60 70 80 90
-5 -10 -15 -20 -25 -30 -35 -40 -45
dB
4L
3L
2L
1L
1R
2R
3R
4R
BUTLER MATRIX ANTENNA
RADIATION PATTERNS
8 element linear array
uniform distribution
spacing 0.5 λ
element pattern E=cos θ
DOA TECHNIQUE # 1

FIGURE 1.4-6

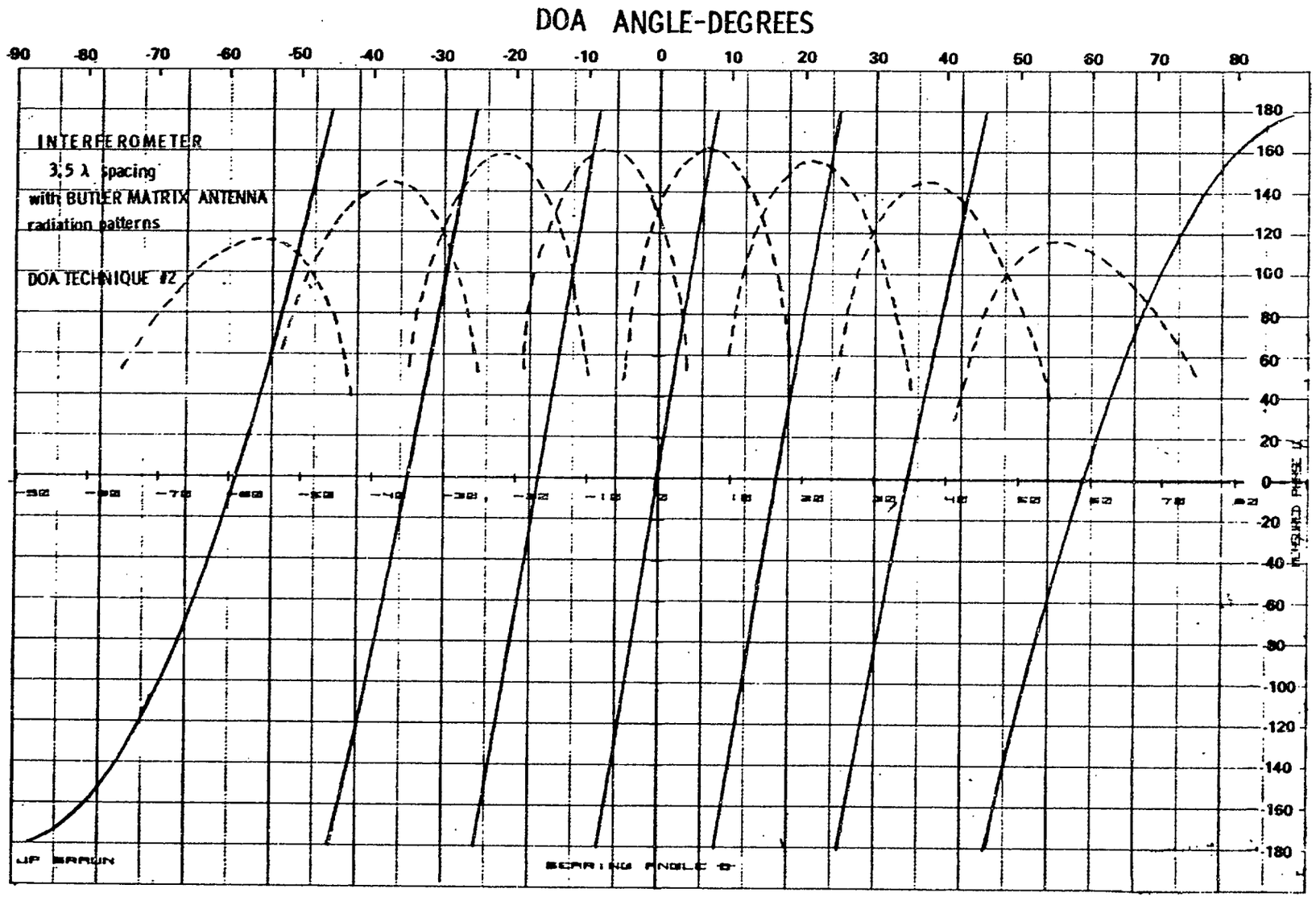
DOA ANGLE-DEGREES
INTERFEROMETER
3.5 λ spacing
with BUTLER MATRIX ANTENNA
radiation patterns
DOA TECHNIQUE #2
-90 -80 -70 -60 -50 -40 -30 -20 -10 0 10 20 30 40 50 60 70 80
180 160 140 120 100 80 60 40 20 0 -20 -40 -60 -80 -100 -120 -140 -160 -180
Φ
UP BRAUN

FIGURE 1.4-7

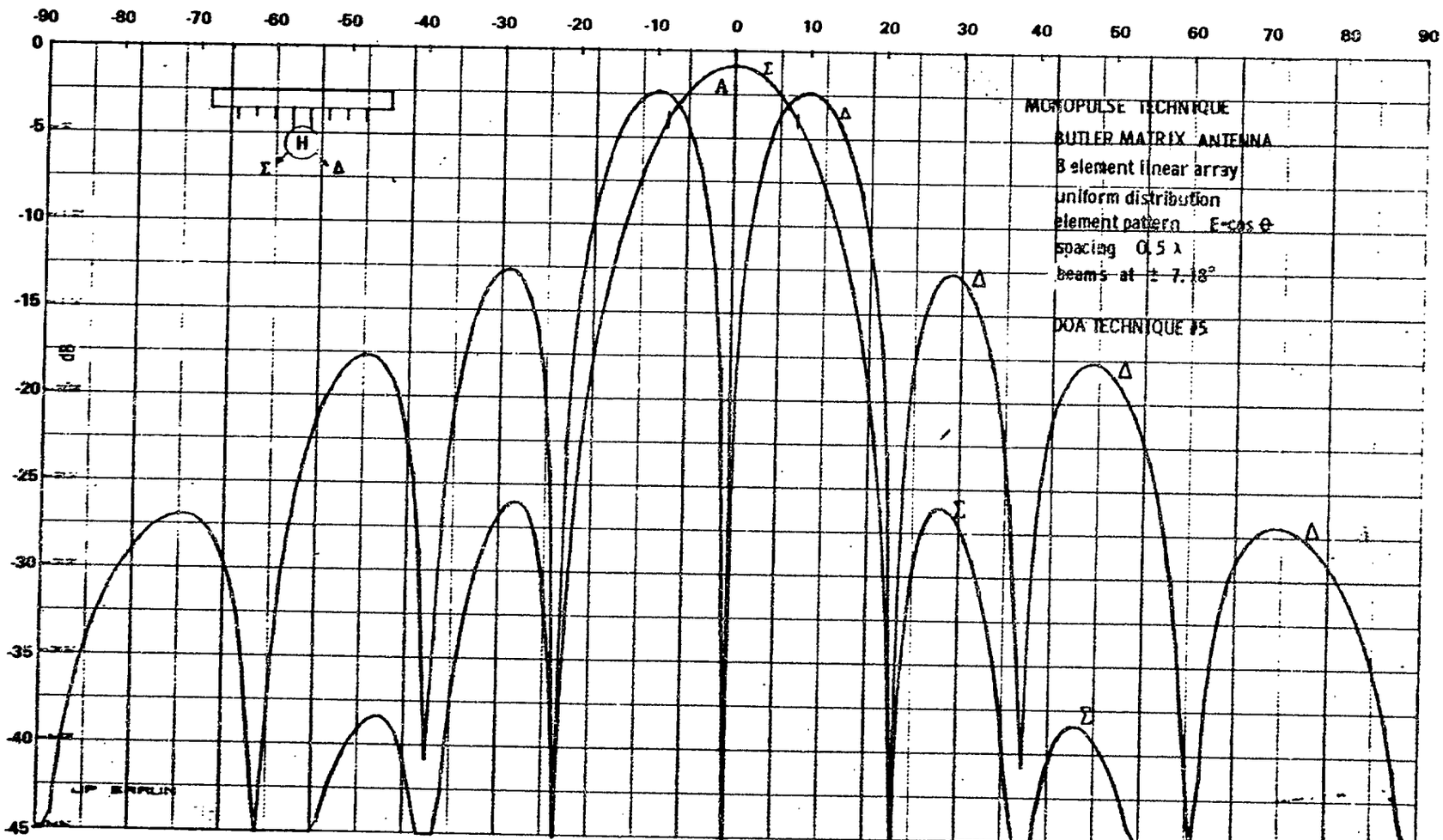
ANGLE DEGREES
-90 -80 -70 -60 -50 -40 -30 -20 -10 0 10 20 30 40 50 60 70 80 90
0 -5 -10 -15 -20 -25 -30 -35 -40 -45
dB
H
Σ
Δ
MONOPULSE TECHNIQUE
BUTLER MATRIX ANTENNA
8 element linear array
uniform distribution
element pattern E=cos θ
spacing 0.5 λ
beams at ± 7.18°
DOA TECHNIQUE #5

FIGURE 1.4-8

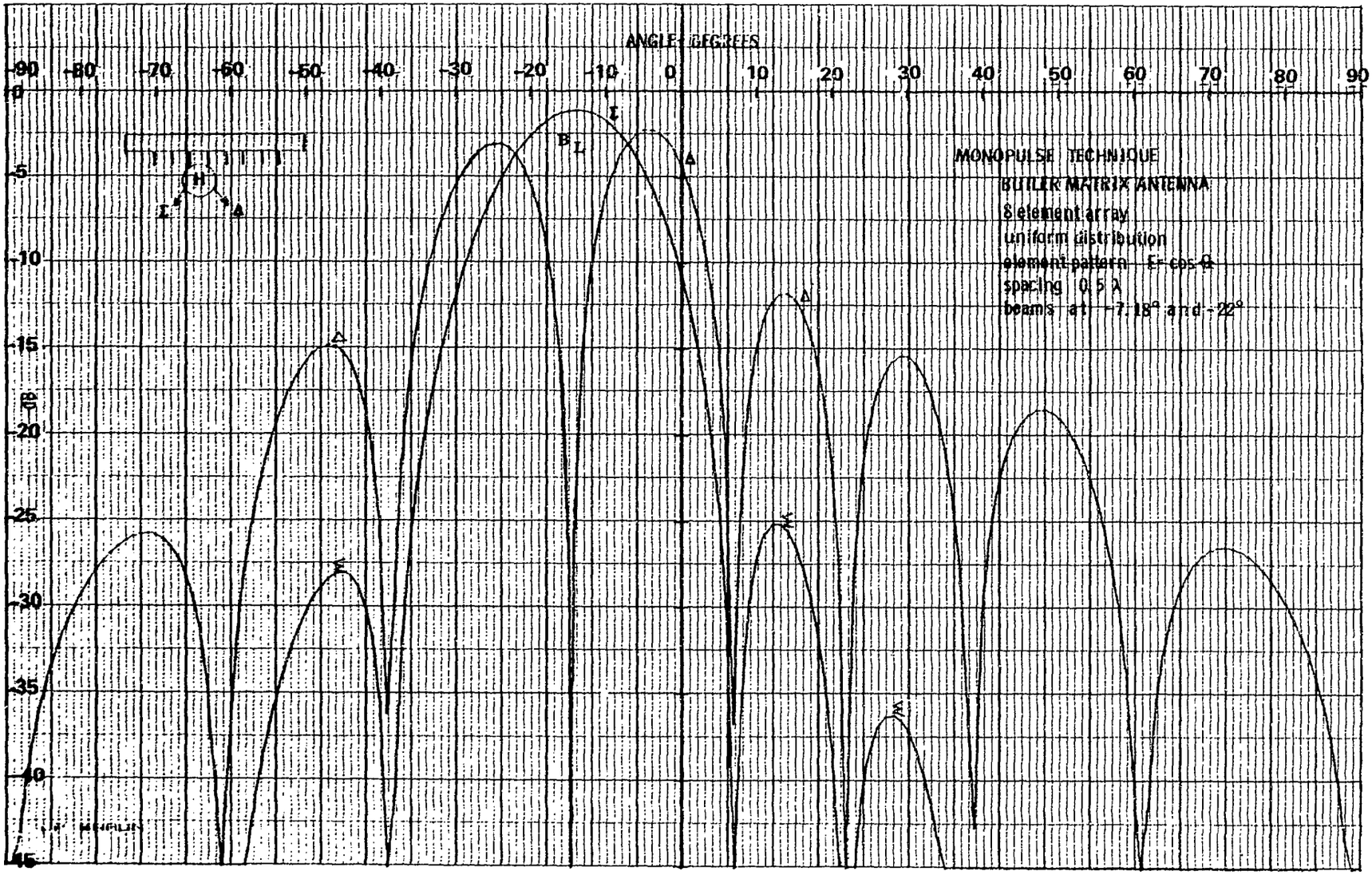
ANGLE - DEGREES
-90 -80 -70 -60 -50 -40 -30 -20 -10 0 10 20 30 40 50 60 70 80 90
0
-5
-10
-15
-20
-25
-30
-35
-40
-45
dB
Σ
Δ
B_L
MONOPULSE TECHNIQUE
BUTLER MATRIX ANTENNA
8 element array
uniform distribution
element pattern E= cos θ
spacing 0.5 λ
beams at -7.18° and -22°

FIGURE 1.4-9

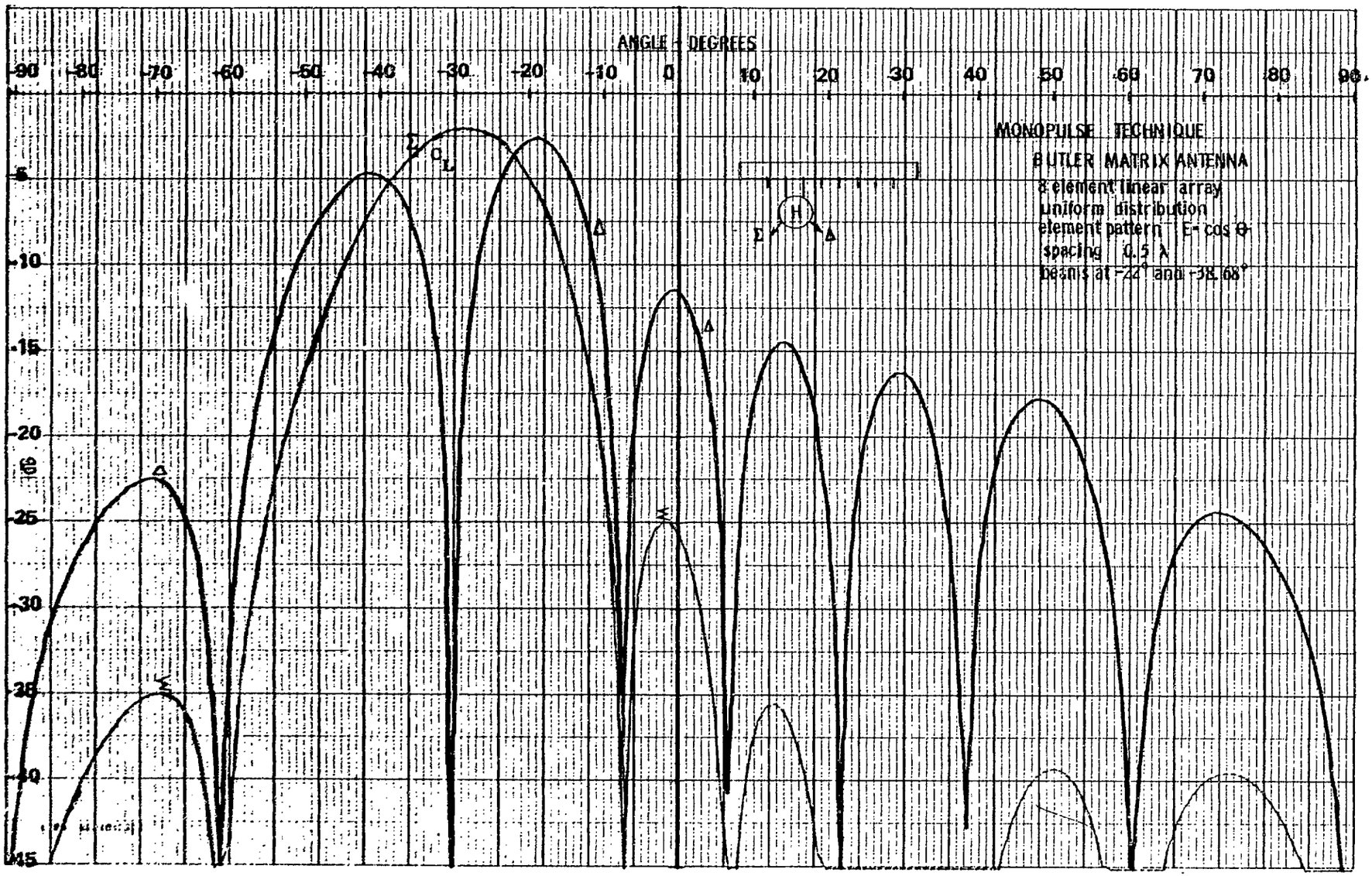

29
0180-24987-1

FIGURE 1.4-10

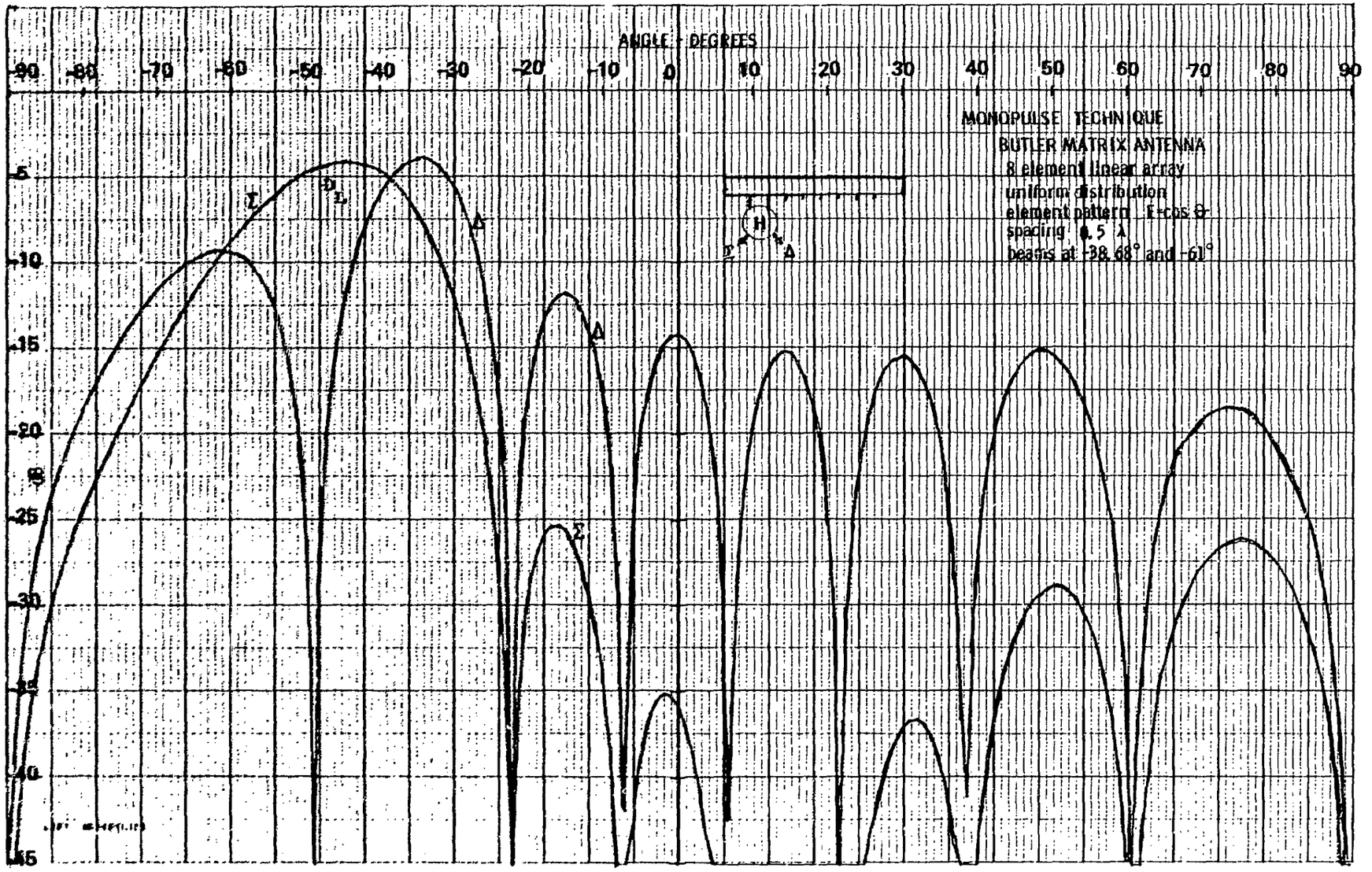
ANGLE - DEGREES
-90 -80 -70 -60 -50 -40 -30 -20 -10 0 10 20 30 40 50 60 70 80 90
-5
-10
-15
-20
-25
-30
-40
-45
MONOPULSE TECHNIQUE
BUTLER MATRIX ANTENNA
8 element linear array
uniform distribution
element pattern E=cos θ
spacing 0.5 λ
beams at -38.68° and -61°
Σ
Δ
H
Σ
Δ

FIGURE 1.4-11

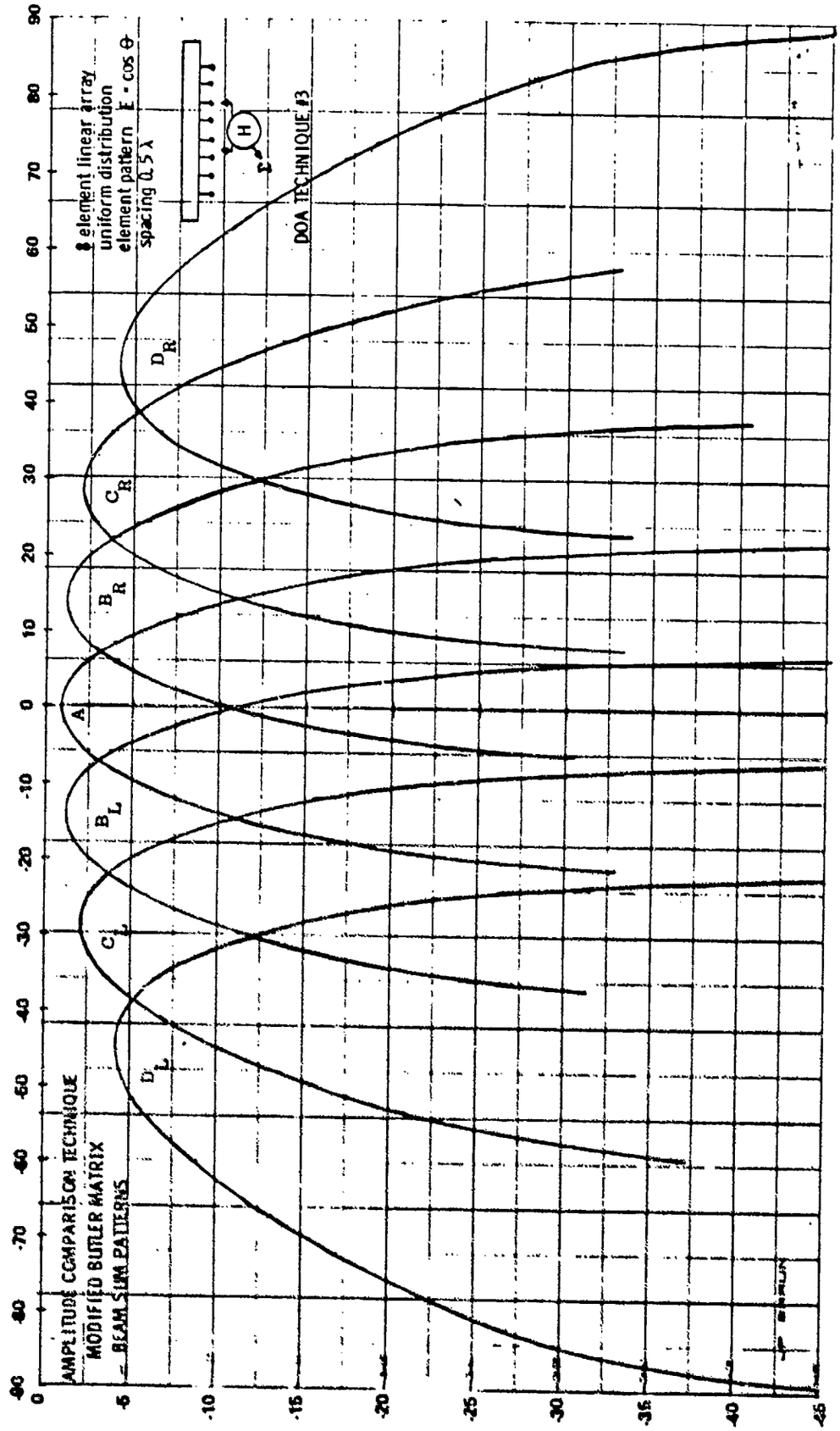
AMPLITUDE COMPARISON TECHNIQUE
MODIFIED BUTLER MATRIX
BEAM SUM PATTERNS
8 element linear array
uniform distribution
element pattern E = cos θ
spacing 0.5 λ
DOA TECHNIQUE #3
A
B_R
C_R
D_R
B_L
C_L
D_L
H
Σ

FIGURE 1.4-12

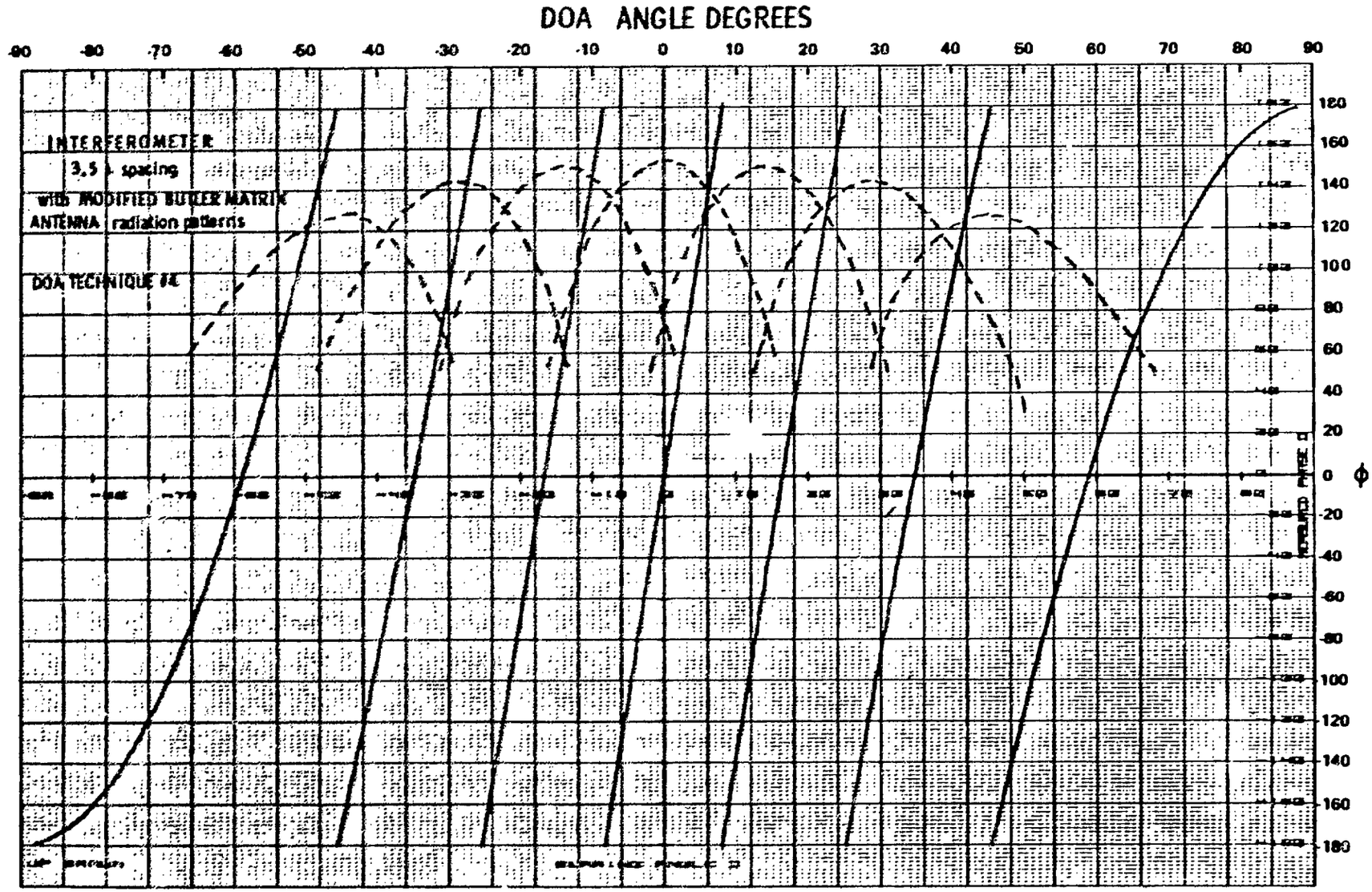
DOA ANGLE DEGREES
-90 -80 -70 -60 -50 -40 -30 -20 -10 0 10 20 30 40 50 60 70 80 90
INTERFEROMETER
3,5 λ spacing
with MODIFIED BUTLER MATRIX
ANTENNA radiation patterns
DOA TECHNIQUE #4
180 160 140 120 100 80 60 40 20 0 -20 -40 -60 -80 -100 -120 -140 -160 -180
ϕ

FIGURE 1.4-13

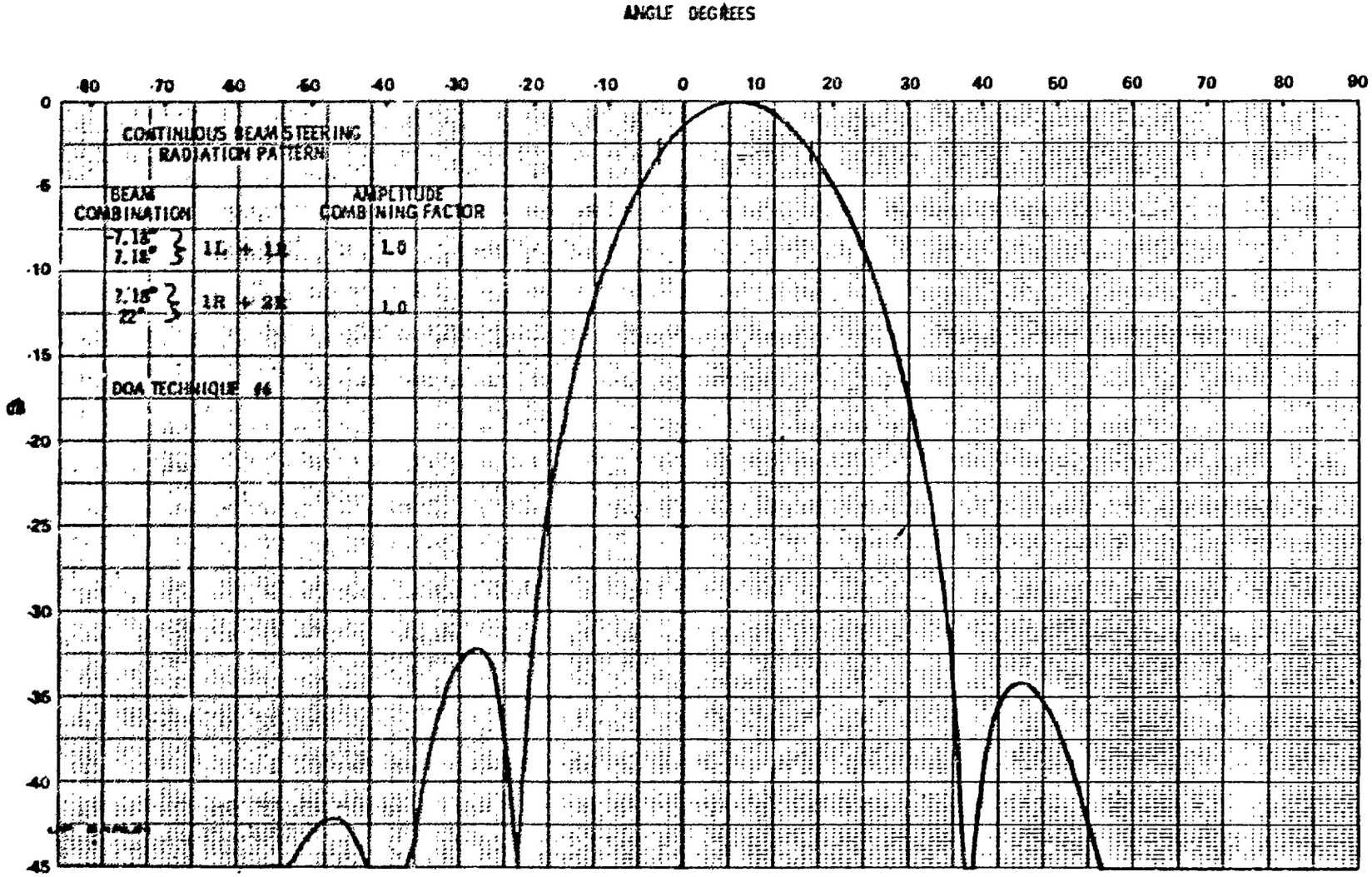
ANGLE DEGREES
-80 -70 -60 -50 -40 -30 -20 -10 0 10 20 30 40 50 60 70 80 90
0 -5 -10 -15 -20 -25 -30 -35 -40 -45
dB
CONTINUOUS BEAM STEERING
RADIATION PATTERN
BEAM COMBINATION
AMPLITUDE COMBINING FACTOR
-7.18° 7.18° 1L + 1R 1.0
7.18° 22° 1R + 2R 1.0
DOA TECHNIQUE #6

FIGURE 1.4-14

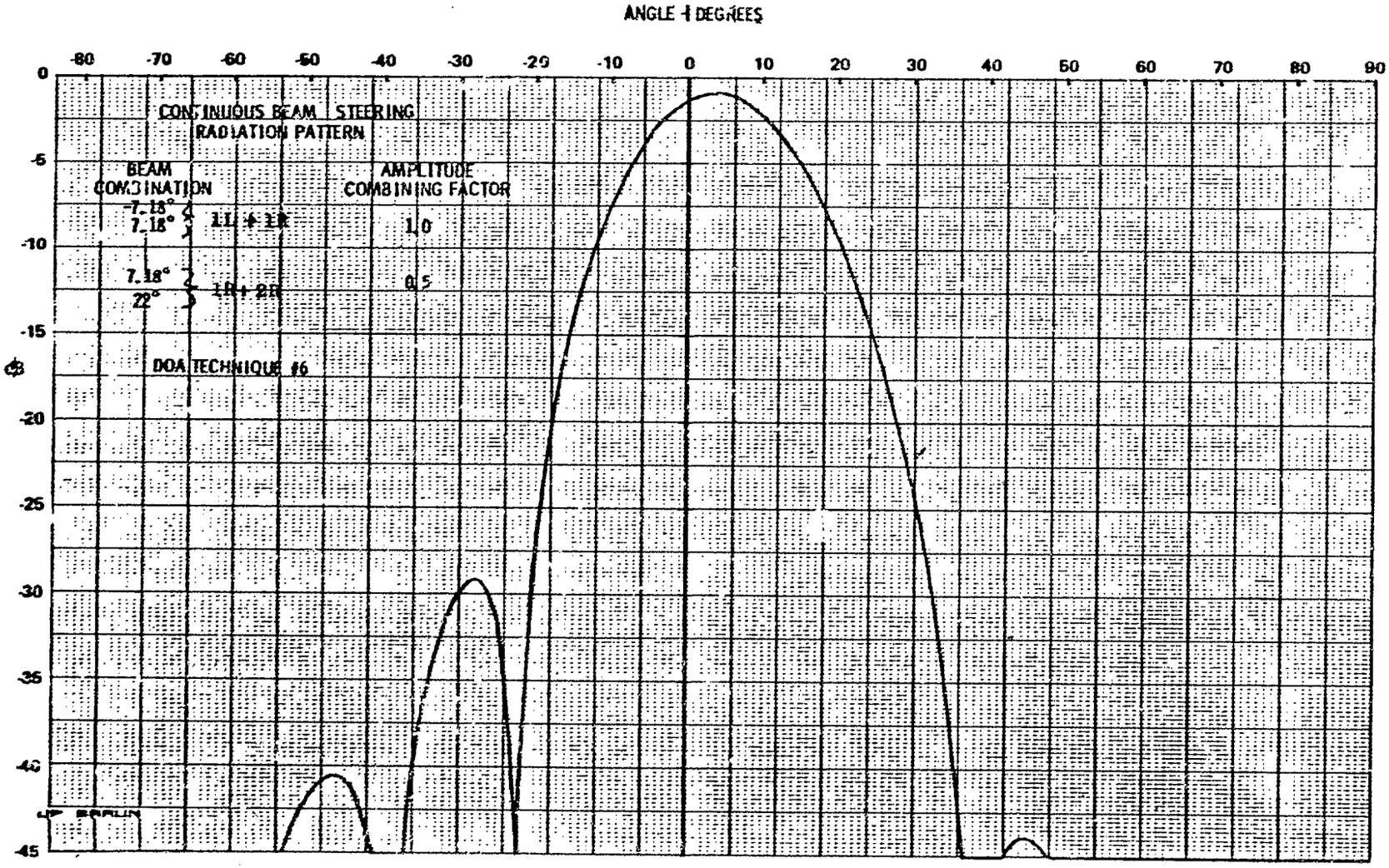
ANGLE - DEGREES
-80 -70 -60 -50 -40 -30 -20 -10 0 10 20 30 40 50 60 70 80 90
0 -5 -10 -15 -20 -25 -30 -35 -40 -45
dB
CONTINUOUS BEAM STEERING
RADIATION PATTERN
BEAM COMBINATION
AMPLITUDE COMBINING FACTOR
-7.18° 1
7.18° 2
1.0
7.18° 2
22° 3
0.5
DOA TECHNIQUE #6

FIGURE 1.4-15

CONTINUOUS BEAM STEERING NETWORK

$V_o(\cos^e\theta_{B1})\cos^{n1}(\theta-\theta_{B1})$

$V_o(\cos^e\theta_{B2})\cos^{n2}(\theta-\theta_{B2})$

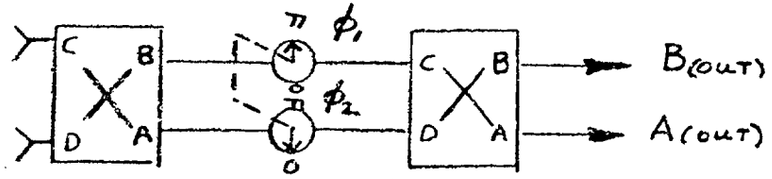

Let input ports C & D be connected to a pair of adjacent beam ports on a multibeam antenna.

where $\cos^e\theta$ = element pattern

θ_B = boresight angle off normal

$$n = \frac{-0.15}{\log\left[\cos\left(\frac{HPBW}{2}\right)\right]}$$

V_o = broadside voltage

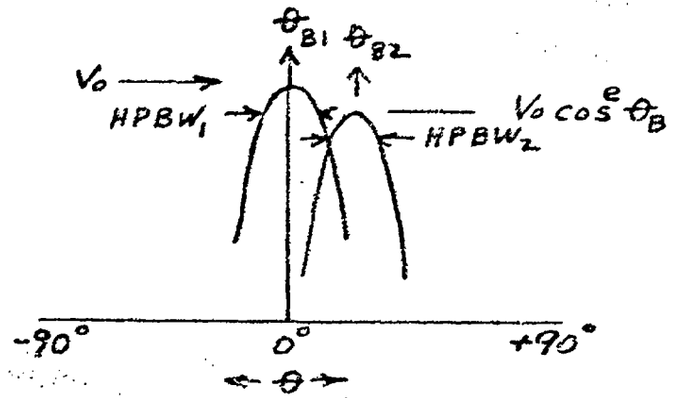

$$A_{OUT} = \left\{\cos^e\theta_{B1}\cos^{n1}(\theta-\theta_{B1})\sin\phi_1 - \cos^e\theta_{B2}\cos^{n2}(\theta-\theta_{B2})\cos\phi_1\right\}$$

$$B_{OUT} = \left\{\cos^e\theta_{B1}\cos^{n1}(\theta-\theta_{B1})\cos\phi_1 + \cos^e\theta_{B2}\cos^{n2}(\theta-\theta_{B2})\sin\phi_1\right\}$$

FIGURE 1.4-16

CBS NETWORK
DOA RESPONSE CHARACTERISTICS (VOLTAGE)

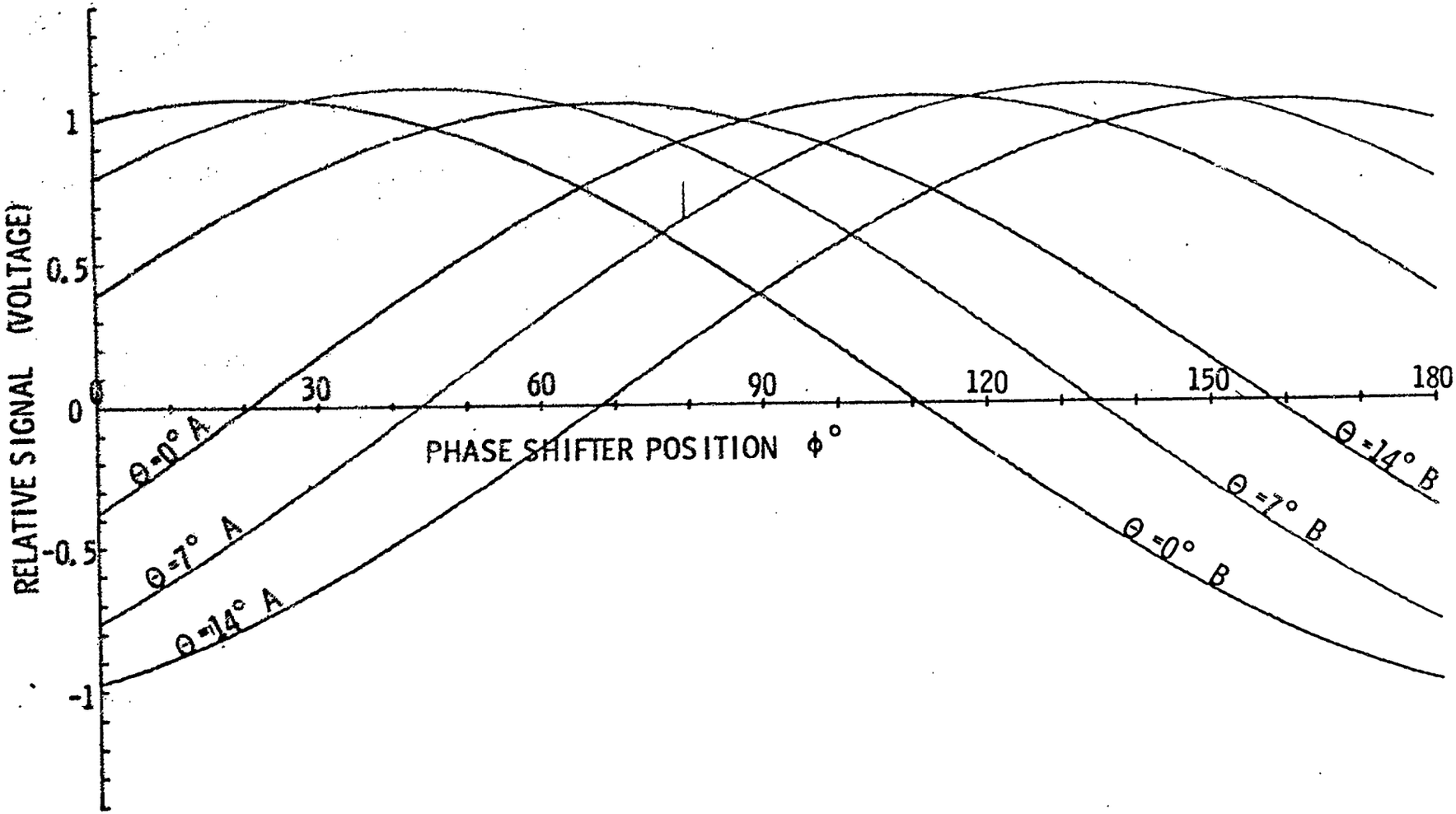

FIGURE 1.4-17

0180-2487-1

CBS NETWORK
DOA RESPONSE CHARACTERISTICS (dB)

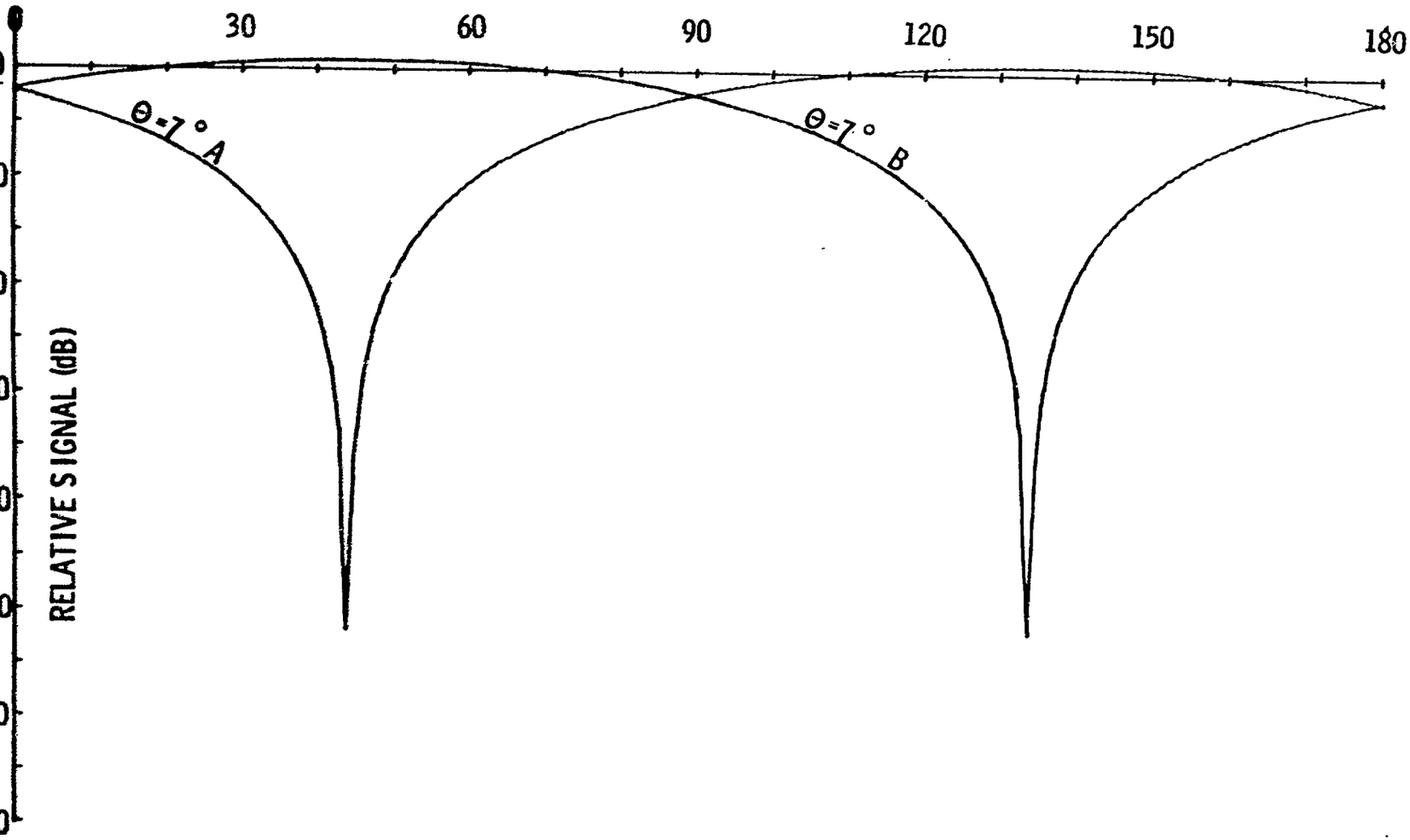

37
D180-24987-1

FIGURE 1.4-18

CBS NETWORK
DOA RESPONSE CHARACTERISTICS (dB)

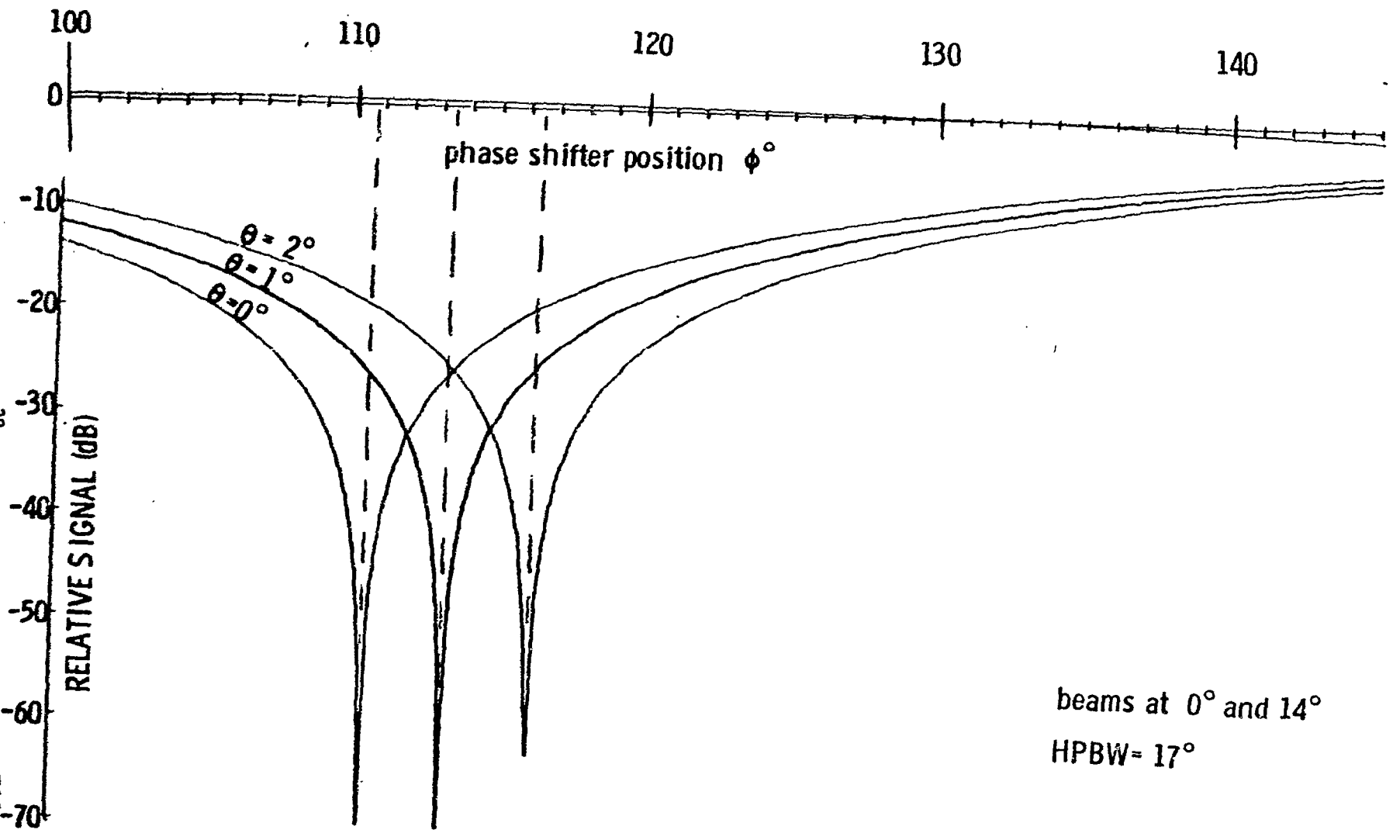

beams at 0° and 14°
HPBW = 17°

D180-24987-1
38

FIGURE 1.4-19

CBS NETWORK
DOA RESPONSE CHARACTERISTICS (dB)

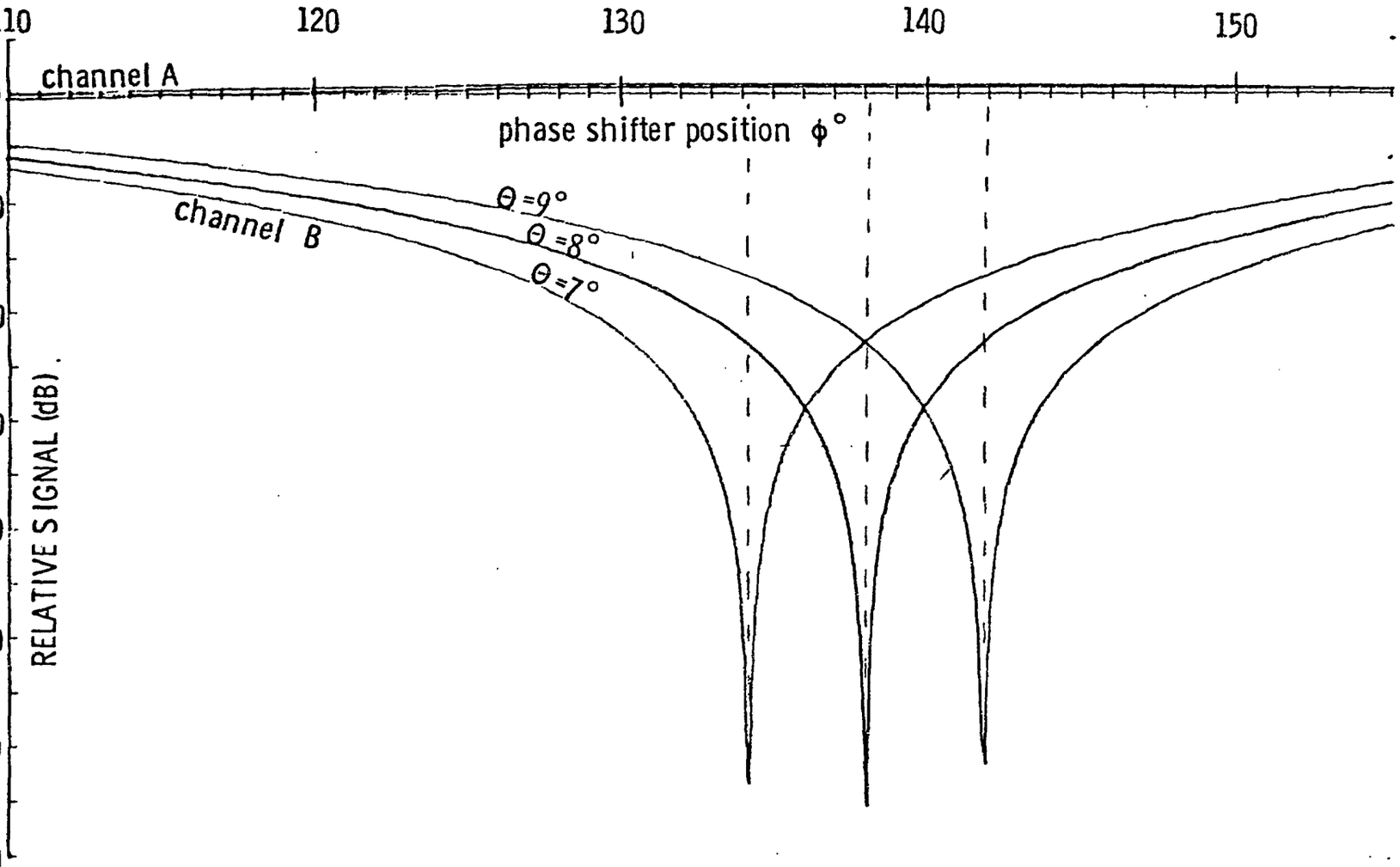

D180-24987-1

FIGURE 1.4-20

CONTINUOUS BEAM STEERING NETWORK

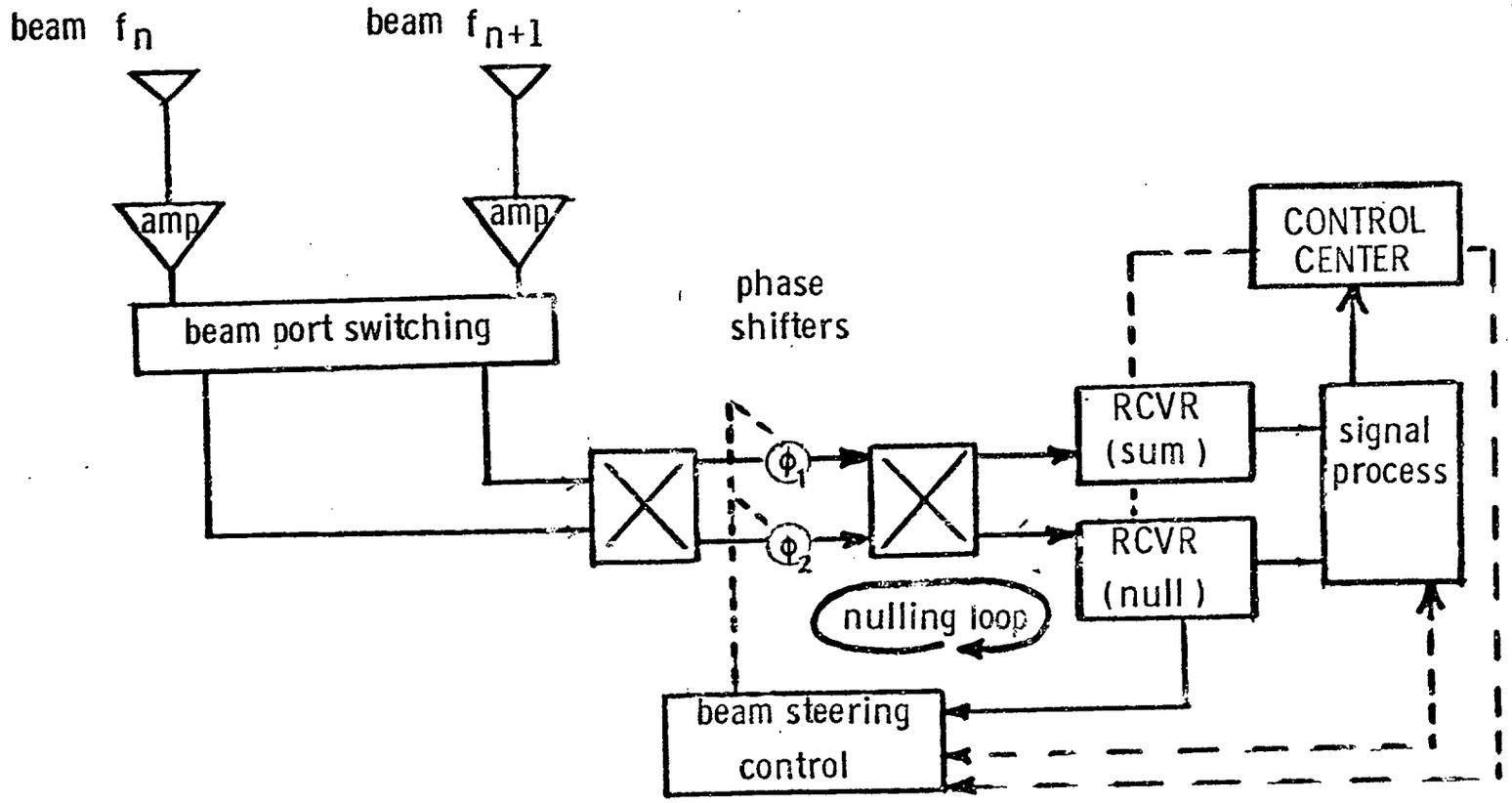

FIGURE 1.4-21

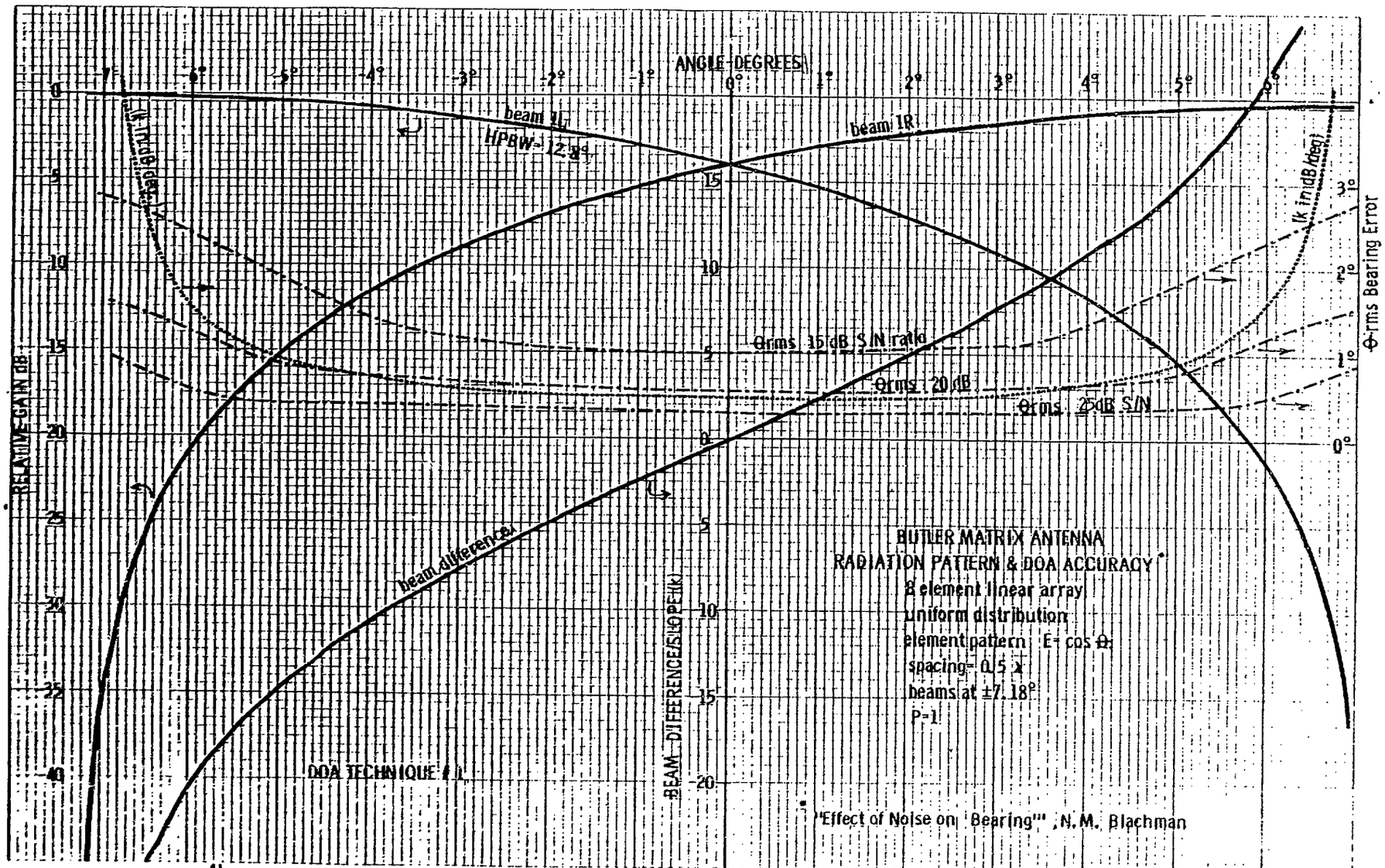

41
D180-24987-1

FIGURE 1.4-22

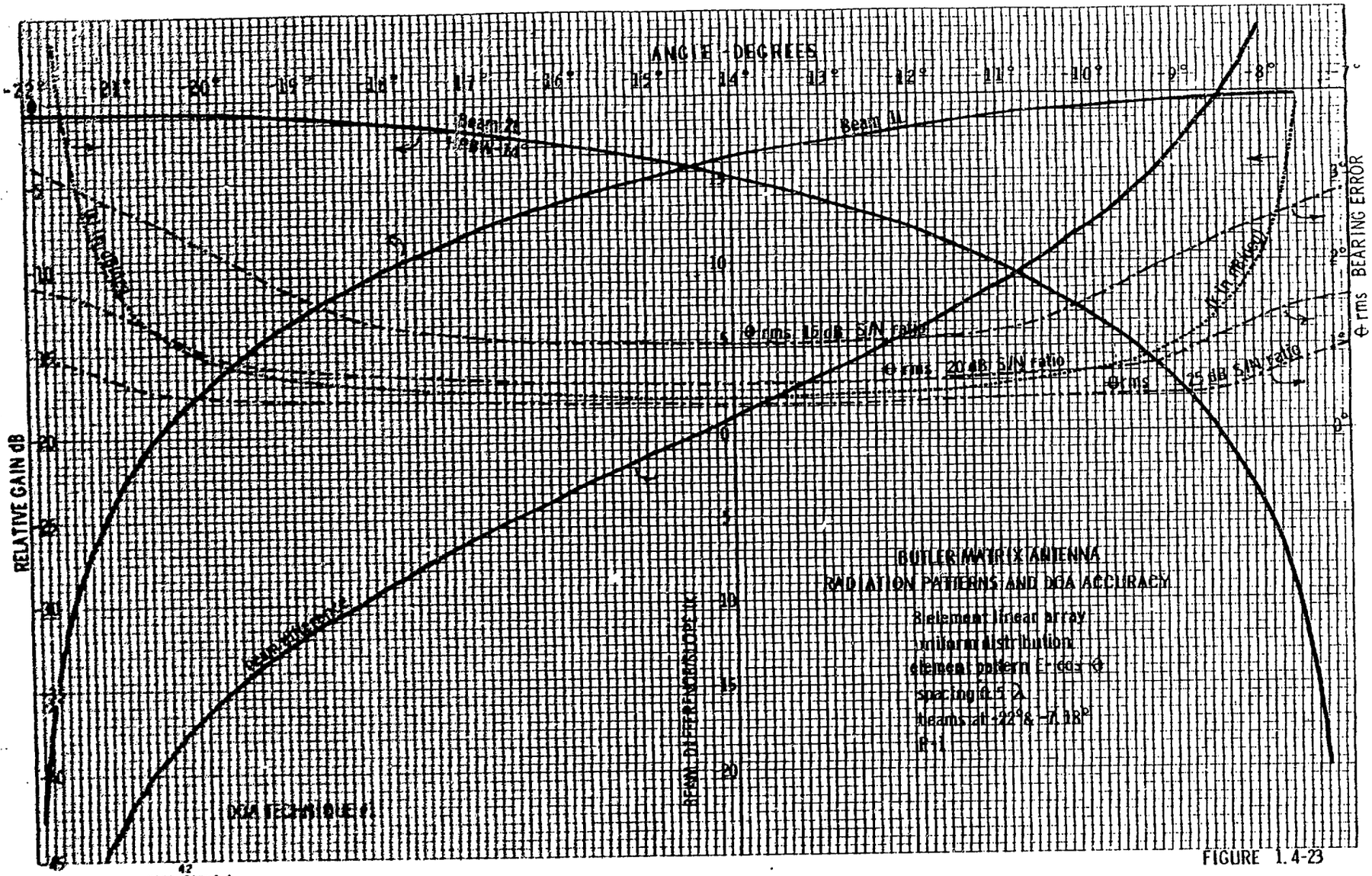
ANGLE - DEGREES
RELATIVE GAIN dB
BEAM DIFFERENCE SLOPE
Φ rms BEARING ERROR
Beam 2R
Beam 1L
Φ rms 10 dB S/N ratio
Φ rms 20 dB S/N ratio
Φ rms 25 dB S/N ratio
BUTLER MATRIX ANTENNA
RADIATION PATTERNS AND DOA ACCURACY
8 element linear array
uniform distribution
element pattern
spacing 0.5 λ
beams at +22° & -11.38°
R-1
42
0180-24982-1

FIGURE 1.4-23

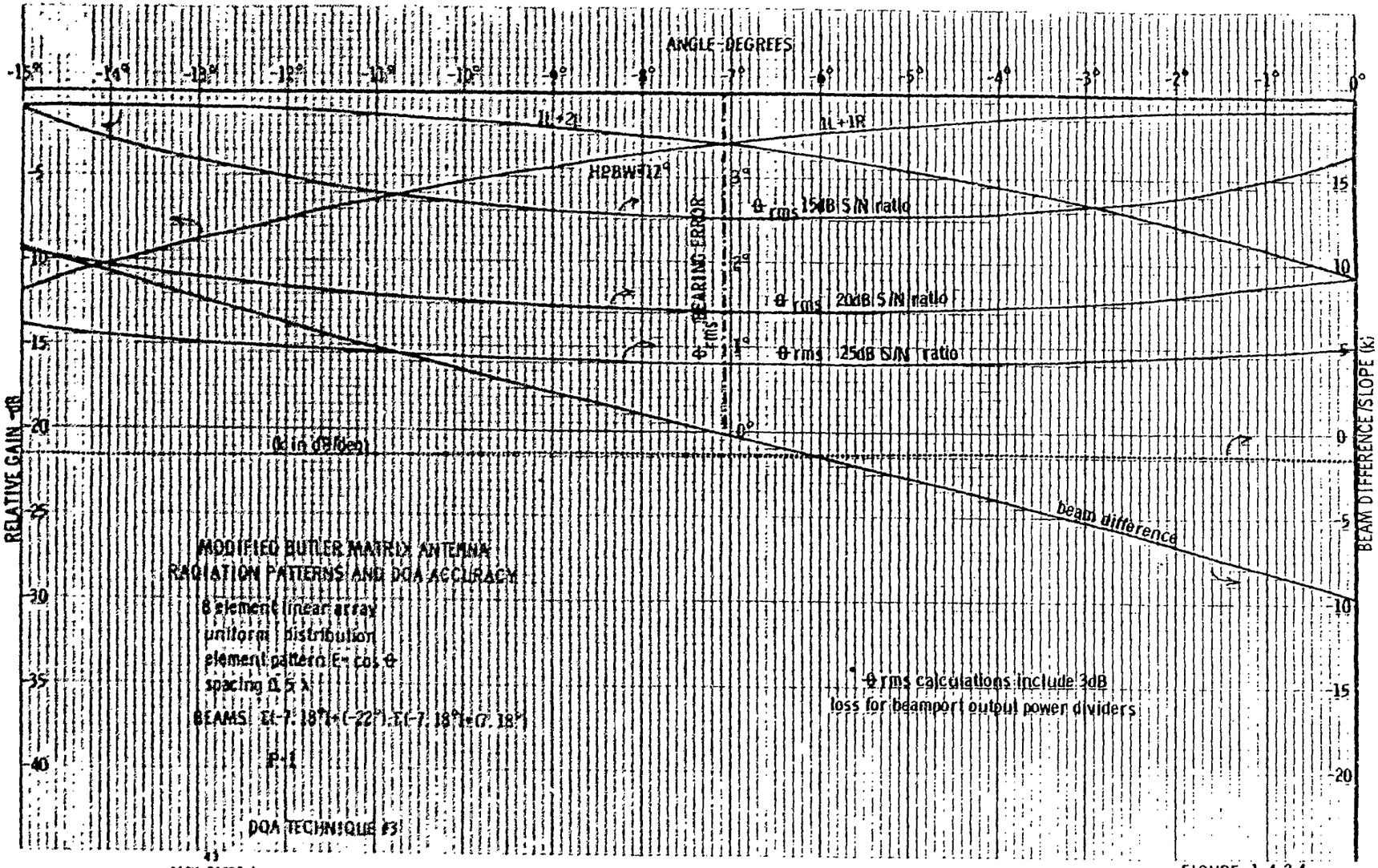

D180-24987-1

FIGURE 1.4-24

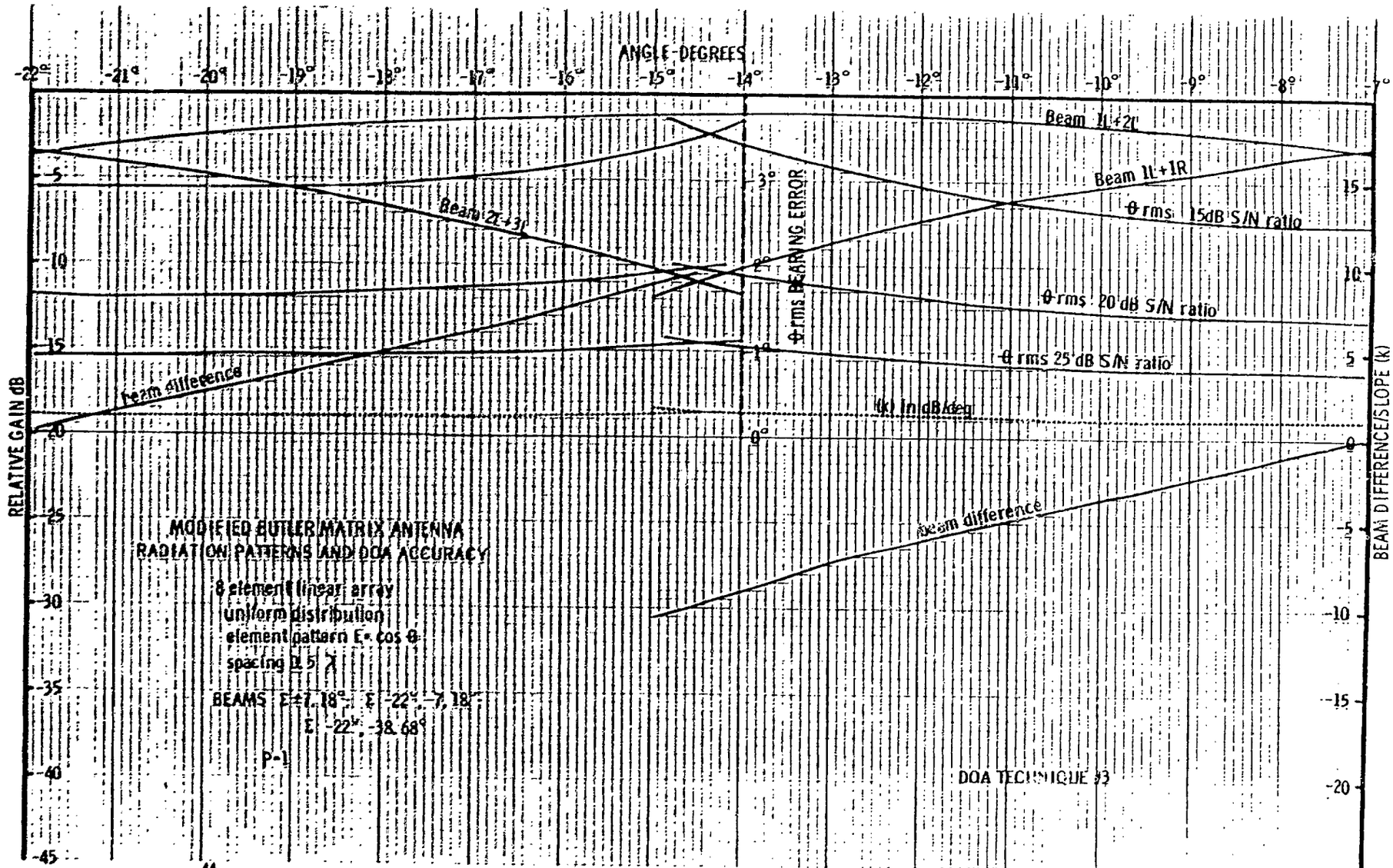
ANGLE-DEGREES
-22°
-21°
-20°
-19°
-18°
-17°
-16°
-15°
-14°
-13°
-12°
-11°
-10°
-9°
-8°
-7°
Beam 1L+2L
Beam 1L+1R
Beam 2L+3L
θ rms 15dB S/N ratio
θ rms 20 dB S/N ratio
θ rms 25 dB S/N ratio
θ rms BEARING ERROR
3°
2°
1°
0°
beam difference
(k) in dB/deg
beam difference
RELATIVE GAIN dB
BEAM DIFFERENCE/SLOPE (k)
-5
-10
-15
-20
-25
-30
-35
-40
-45
5
0
-5
-10
-15
-20
MODIFIED BUTLER MATRIX ANTENNA
RADIATION PATTERNS AND DOA ACCURACY
8 element linear array
uniform distribution
element pattern E = cos θ
spacing 0.5 λ
BEAMS Σ ±7.18°, Σ -22°, -7, 18°
Σ -22°, -38.68°
P-1
DOA TECHNIQUE #3
47 0700
K-E
44
0180-24987-1

FIGURE 1.4-25

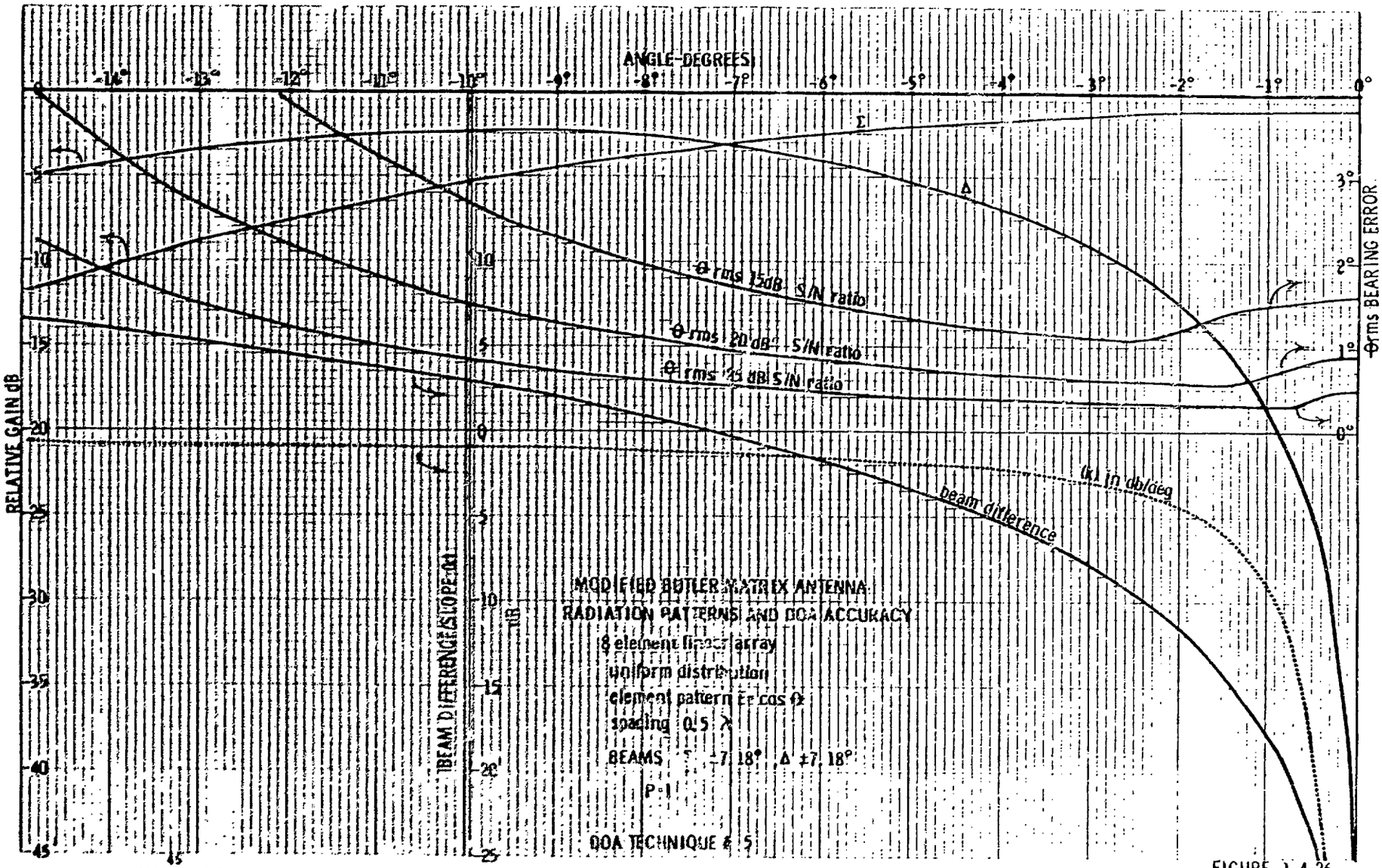
ANGLE-DEGREES
-14°
-13°
-12°
-11°
-10°
-9°
-8°
-7°
-6°
-5°
-4°
-3°
-2°
-1°
0°
Σ
Δ
θ rms 15dB S/N ratio
θ rms 20 dB S/N ratio
θ rms 25 dB S/N ratio
(k) in db/deg
beam difference
RELATIVE GAIN dB
BEAM DIFFERENCE SLOPE dB
θrms BEARING ERROR
MODIFIED BUTLER MATRIX ANTENNA
RADIATION PATTERNS AND DOA ACCURACY
8 element linear array
uniform distribution
element pattern ~ cos θ
spacing 0.5 λ
BEAMS Σ -7.18°, Δ +7.18°
P=1
DOA TECHNIQUE # 5
0180-24987-1

FIGURE 1.4-26

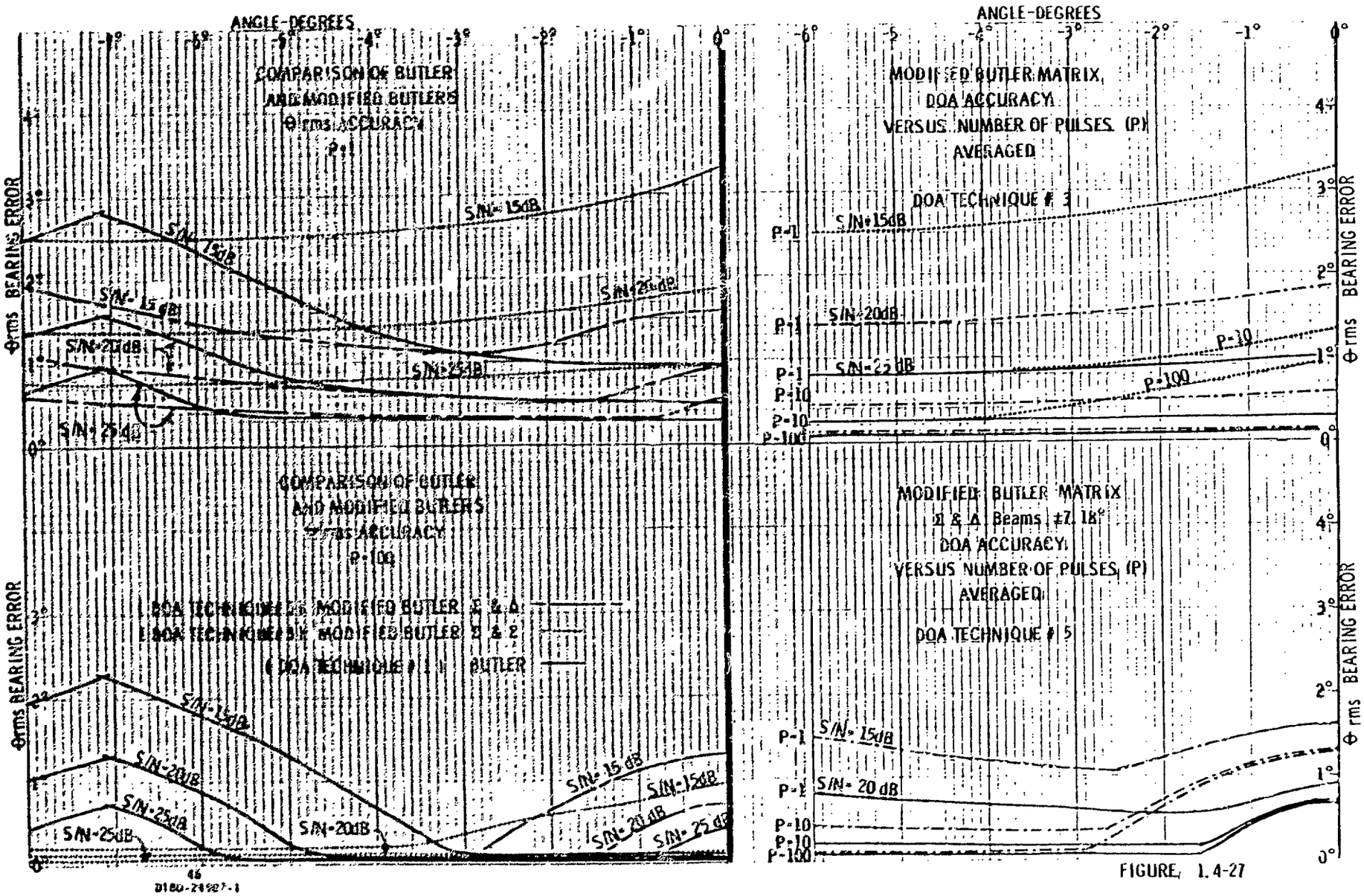
ANGLE-DEGREES
COMPARISON OF BUTLER AND MODIFIED BUTLERS
θ rms ACCURACY
P=1
S/N=15dB
S/N=20dB
S/N=25dB
θ rms BEARING ERROR
COMPARISON OF BUTLER AND MODIFIED BUTLERS
θ rms ACCURACY
P=100
DOA TECHNIQUE # 3 MODIFIED BUTLER Σ & Δ
DOA TECHNIQUE # 4 MODIFIED BUTLER Σ & Σ
DOA TECHNIQUE # 1 BUTLER
S/N=15dB
S/N=20dB
S/N=25dB
MODIFIED BUTLER MATRIX
DOA ACCURACY
VERSUS NUMBER OF PULSES (P)
AVERAGED
DOA TECHNIQUE # 3
P=1
P=10
P=100
MODIFIED BUTLER MATRIX
Σ & Δ Beams ±7.18°
DOA ACCURACY
VERSUS NUMBER OF PULSES (P)
AVERAGED
DOA TECHNIQUE # 5

FIGURE 1.4-27

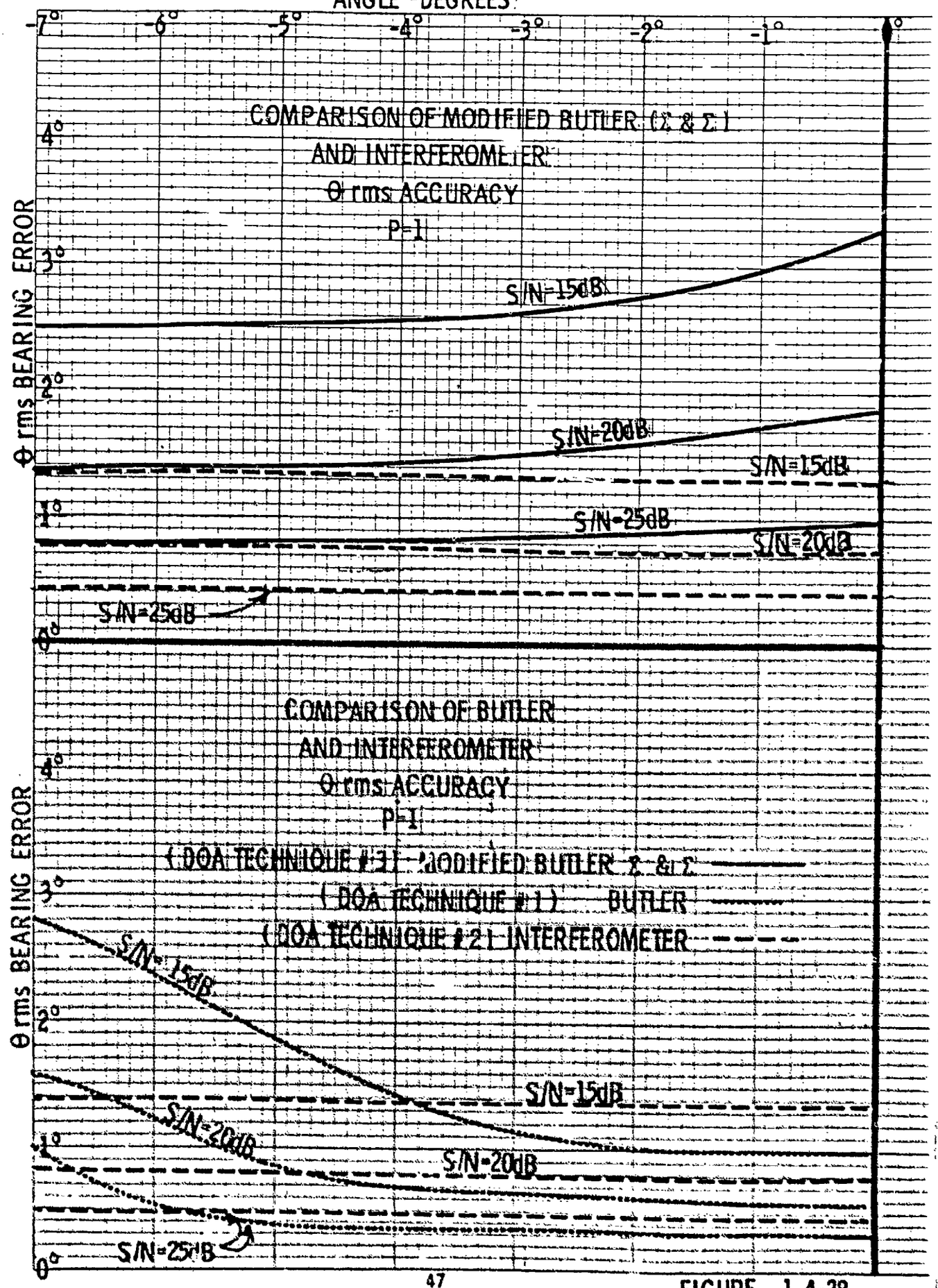

47 0700

K-E 10 X 10 TO THE INCH • 4 X 10 INCHES
KEUFFEL & ESSER CO. MADE IN U.S.A.

FIGURE 1.4-28

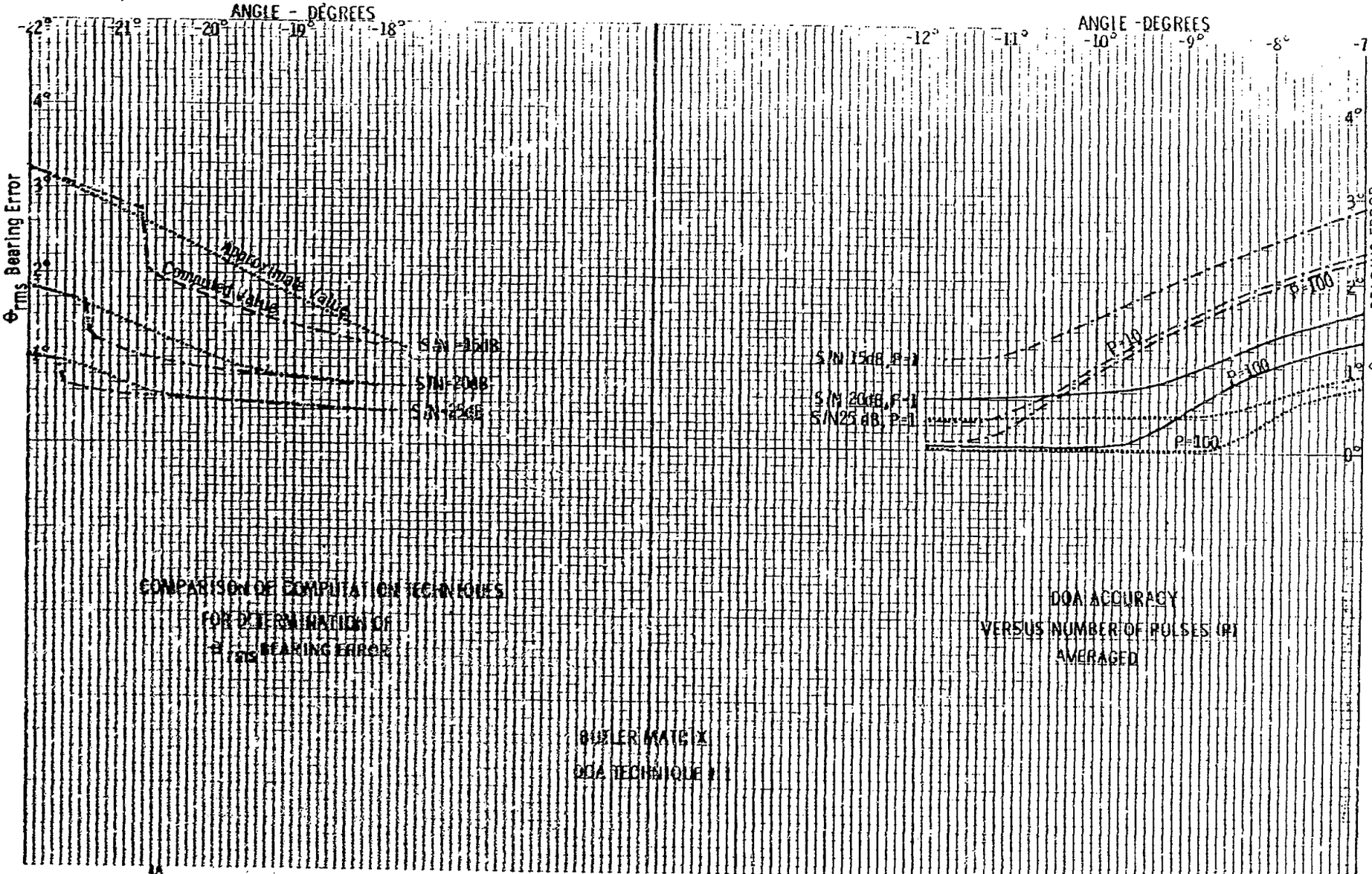
ANGLE - DEGREES
-22°
-21°
-20°
-19°
-18°
ANGLE -DEGREES
-12°
-11°
-10°
-9°
-8°
-7
4°
3°
2°
1°
0°
Φ rms Bearing Error
Φ rms BEARING ERROR
Monotriple (alt)
Combined value
S/N 25dB
S/N 20dB
S/N 15dB
S/N 15dB, P=1
S/N 20dB, P=1
S/N 25 dB, P=1
P=20
P=100
P=100
P=100
COMPARISON OF COMPUTATION TECHNIQUES
FOR DETERMINATION OF
Φ rms BEARING ERROR
BUTLER MATRIX
DOA TECHNIQUE #1
DOA ACCURACY
VERSUS NUMBER OF PULSES (P)
AVERAGED
47 0703
D180-24987-1

FIGURE 1.4-29

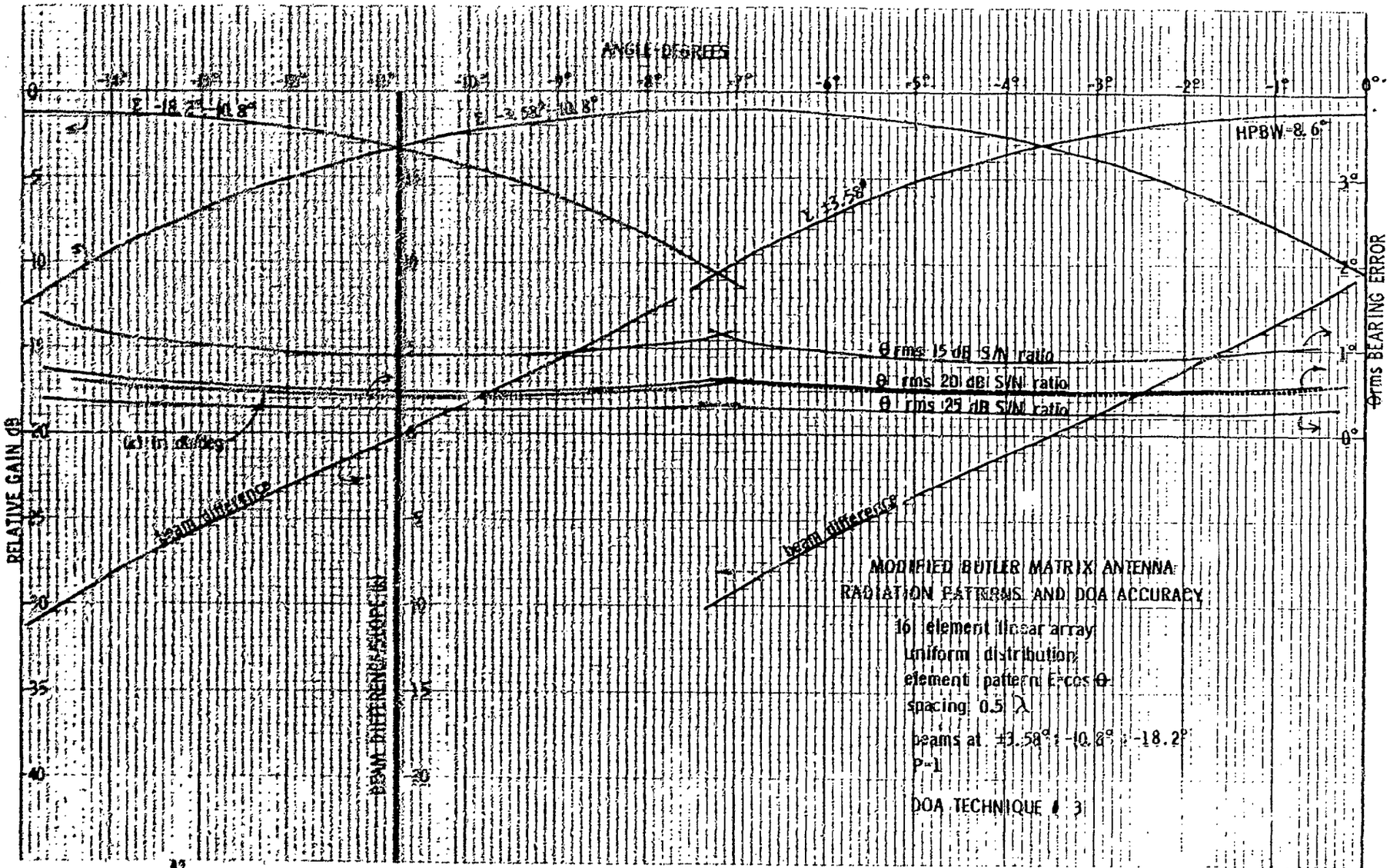
ANGLE-DEGREES
HPBW-8.6°
Σ -18.2°, -10.8°
Σ -3.58°, -10.8°
Δ +3.58°
θ rms 15 dB S/N ratio
θ rms 20 dB S/N ratio
θ rms 25 dB S/N ratio
sum difference
beam difference
RELATIVE GAIN dB
BEAM DIFFERENCE SLOPE (K)
θ rms BEARING ERROR
MODIFIED BUTLER MATRIX ANTENNA
RADIATION PATTERNS AND DOA ACCURACY
16 element linear array
uniform distribution
element pattern f=cos θ
spacing 0.5 λ
beams at ±3.58°, -10.8°, -18.2°
P=1
DOA TECHNIQUE # 3

FIGURE 1.4-30

DERIVATION OF
CONTINUOUS BEAM STEERING NETWORK EQUATIONS

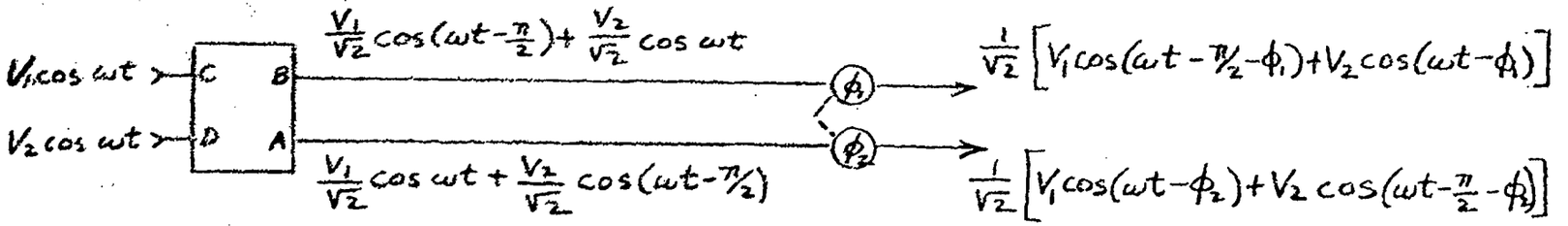

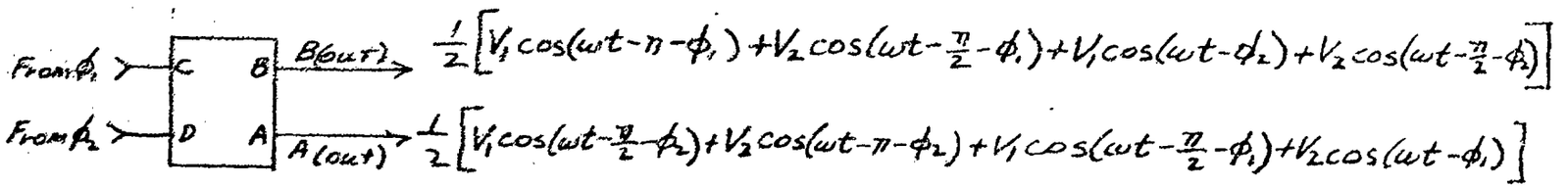

let $\phi_1 + \phi_2 = \pi \Rightarrow \phi_2 = \pi - \phi_1$

$$B(out) = \frac{1}{2} \left\{ V_1 \left[\cos(\omega t - \pi - \phi_1) + \cos(\omega t - \pi + \phi_1) \right] + V_2 \left[\cos(\omega t - \frac{\pi}{2} - \phi_1) + \cos(\omega t - \frac{3\pi}{2} + \phi_1) \right] \right\} \quad (1)$$

$$A(out) = \frac{1}{2} \left\{ V_1 \left[\cos(\omega t - \frac{3\pi}{2} + \phi_1) + \cos(\omega t - \frac{\pi}{2} - \phi_1) \right] + V_2 \left[\cos(\omega t - 2\pi + \phi_1) + \cos(\omega t - \phi_1) \right] \right\} \quad (2)$$

Appendix 3.1

THE BOEING COMPANY
SEATTLE, WASHINGTON

Expanding Eqn's (1) & (2) yields

$$B_{(OUT)} = \frac{1}{2}\left\{V_1\left[\cos(\omega t-\pi)\cos\phi_1+\sin(\omega t-\pi)\sin\phi_1+\cos(\omega t-\pi)\cos\phi_1-\sin(\omega t-\pi)\sin\phi_1\right]\right.$$
$$\left.+V_2\left[\cos(\omega t-\tfrac{\pi}{2})\cos\phi_1+\sin(\omega t-\tfrac{\pi}{2})\sin\phi_1+\cos(\omega t-\tfrac{3\pi}{2})\cos\phi_1-\sin(\omega t-\tfrac{3\pi}{2})\sin\phi_1\right]\right\}$$

$$B_{(OUT)} = \frac{1}{2}\left\{V_1\left[-2\cos(\omega t)\cos\phi_1\right]+V_2\left[-2\cos(\omega t)\sin\phi_1\right]\right\} \qquad (3)$$

$$A_{(OUT)} = \frac{1}{2}\left\{V_1\left[\cos(\omega t-\tfrac{3\pi}{2})\cos\phi_1-\sin(\omega t-\tfrac{3\pi}{2})\sin\phi_1+\cos(\omega t-\tfrac{\pi}{2})\cos\phi_1+\sin(\omega t-\tfrac{\pi}{2})\sin\phi_1\right]\right.$$
$$\left.+V_2\left[\cos(\omega t+\phi_1)+\cos(\omega t-\phi_1)\right]\right\}$$

$$A_{(OUT)} = \frac{1}{2}\left\{V_1\left[-2\cos(\omega t)\sin\phi_1\right]+V_2\left[2\cos(\omega t)\cos\phi_1\right]\right\} \qquad (4)$$

$$A_{(OUT)} = -\left[V_1\sin\phi_1-V_2\cos\phi_1\right]\cos(\omega t) \qquad B_{(OUT)} = -\left[V_1\cos\phi_1+V_2\sin\phi_1\right]\cos\omega t \qquad (5)\&(6)$$

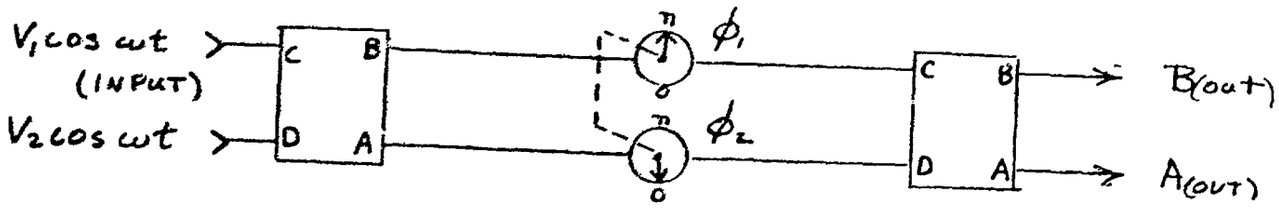

Let the input ports C & D be connected to a pair of adjacent beam ports on a multi-beam antenna*. The voltage (V) response patterns being represented by the form —

$$V_{1,2} = V_0 [\cos^e \theta_B] \cos^n (\theta - \theta_B) \quad (7)$$ where $\cos^e \theta$ = array element pattern

θ_B = boresight angle off normal

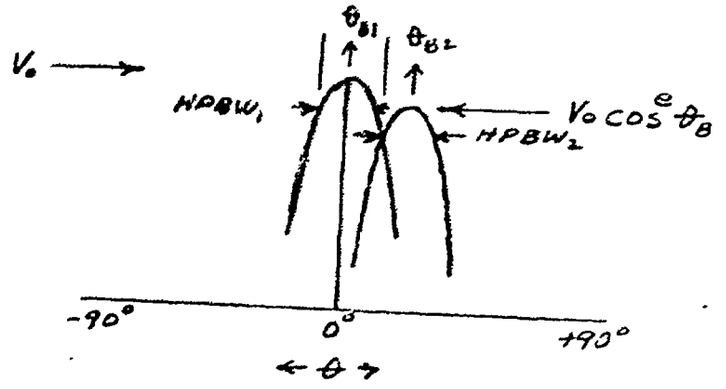

$$n = \frac{-.15}{\log\left[\cos\left(\frac{HPBW}{2}\right)\right]}$$

V_0 = broadside voltage response

* INPUTS ARE IN PHASE

Substituting (7) into (5) & (6), neglecting the (−) sign, let $V_0 = 1$, $t = 0$, then

$$A_{out} = \left\{ \cos^{e}\theta_{B1} \cos^{n_1}(\theta - \theta_{B1}) \sin\phi_1 - \cos^{e}\theta_{B2} \cos^{n_2}(\theta - \theta_{B2}) \cos\phi_1 \right\} \qquad (5)'$$

$$B_{out} = \left\{ \cos^{e}\theta_{B1} \cos^{n_1}(\theta - \theta_{B1}) \cos\phi_1 + \cos^{e}\theta_{B2} \cos^{n_2}(\theta - \theta_{B2}) \sin\phi_1 \right\} \qquad (6)'$$

As a special case, let $\phi_1 = \frac{\pi}{2}$, then

$A_{out} = \cos^{e}\theta_{B1} \cos^{n_1}(\theta - \theta_{B1})$ ← The pattern from beam f_n

$B_{out} = \cos^{e}\theta_{B2} \cos^{n_2}(\theta - \theta_{B2})$ ← The pattern from beam f_{n+1}

HP-98CC PROGRAM FOR θ_{rms} APPROXIMATE
(use when S/N < -6dB)

```
0:
 MB MONOPULSE DO
A ACC APPROXIMAT
E"⊢
1:
FXD 3;FLT 3;TBL
1;ENT "LOW THETA
-DEG",R46;ENT "H
IGH THETA-DEG",R
47⊢
2:
ENT "ANG DELTA D
EG",R40⊢
3:
SCL R46,R47,-45,
5⊢
4:
0→R29;ENT "ENT 5
 FOR DIFFAT",R29
⊢
5:
CFG 1;0→R32;ENT
"ENT 9 FOR SECPA
T",R32;IF R32=9;
SFG 1;GTO 16⊢
6:
ENT "COS XP-VOLT
AGE R30",R30⊢
7:
ENT "SPACING R31
",R31⊢
8:
ENT "NUM. ELEM.
R33",R33⊢
9:
ENT "AMP. VALUES
 R(A)"⊢
10:
1→A⊢
11:
"K";ENT RA;RA→R(
R33+1-A)⊢
12:
IF R33/2>A;1+A→A
;GTO "K"⊢
13:
0→R34;1→A⊢
14:
"M";RA→R34+R34⊢
15:
IF R33>A;1+A→A;
GTO "M"⊢
16:
ENT "NU. OF BEAM
S;R35",R35⊢
17:
36→B⊢
18:
"T";ENT R(B)⊢
19:
IF R35+35>B;1+B→
B;GTO "T"⊢
20:
R46→Z⊢
21:
0→R39⊢
22:
"N";0→R41→R42→R4
3⊢
23:
0→A;36→B⊢
24:
"P";A+1→A⊢
25:
"Q";SIN RB→X⊢
26:
360→R31(A-R33/2-
.5)(SIN Z-X)→R44
⊢
27:
RACOS R44+R41→R4
1⊢
28:
RASIN R44+R42→R4
2⊢
29:
IF R29=5;-RA→RA⊢
30:
IF R33>A;GTO "P"
⊢
31:
IF R35+35>B;1+B→
B;1→A;GTO "Q"⊢
32:
COS Z↑R30/R34*
ABS √(R41↑2+R42↑
2)→R43⊢
33:
R43/√R35→R45⊢
34:
IF R32≠9;R45→R(5
1+R39)⊢
```

Appendix 3.2

```
35:
IF R32=9;R45→R(1
01+R39)⊢
36:
PLT Z,20LOG R45⊢
37:
IF R47>Z;R40+Z→Z
;1+R39→R39;GTO "
N"⊢
38:
IF FLG 1;GTO 40⊢
39:
PEN ;GTO 3⊢
40:
PEN ;SCL R46,R47
,-25,25⊢
41:
R46→Z;0→R39⊢
42:
"R";R(101+R39)/R
(51+R39)→R(151+R
39)⊢
43:
PLT Z,20LOG R(15
1+R39,⊢
44:
IF R47>Z;R40+Z→Z
;1+R39→R39;GTO
R"⊢
45:
PEN ;R46→Z;0→R39
⊢
46:
SCL R46,R47,-25,
25⊢
47:
"S";PLT Z+.5R40,
20(LOG R(152+R39
)-LOG R(151+R39)
)/R40⊢
48:
IF R47>Z+R40;R40
+Z→Z;1+R39→R39;
GTO "S"⊢
49:
ENT "S.N-DB";Y;R
46→Z;0→R39;PEN ;
SCL R46,R47,-5,5
;ENT "NU P",R48⊢
50:
"V";(Y+20(LOG (R
(51+R39)+R(52+R3
9))-LOG 2))/10→R
49;1/10↑R49→R49⊢
51:
(Y+20(LOG (R(101
+R39)+R(102+R39)
)-LOG 2))/10→R50
;1/10↑R50→R50⊢
52:
R40/(R(152+R39)-
R(151+R39))→R0⊢
53:
(20/R40)LOG (R(1
51+R39)/R(152+R3
9))→B;ABS B→B⊢
54:
IF R49<.25;IF R5
0<.25;PLT Z+.5R4
0,(8.686/B)Γ((R4
9+R50)/2R48)⊢
55:
Y-6+20(LOG (R(10
1+R39)+R(102+R39
))-.3)→R50;.1R50
→R50⊢
56:
ABS R0Γ(R49/2R48
)→C⊢
57:
IF 0>R50;PLT Z+.
5R40,CΓ(1+1.57R4
8(1-10↑R50)↑2)⊢
58:
IF R47>Z+R40;R40
+Z→Z;1+R39→R39;
GTO "V"⊢
59:
END ⊢
R208
```

Appendix 3.2

```
PRT "MB ANT. PAT
. PLOT"⊢
1:
FIX 3;PLT 3;TBL
1;ENT "LOW THETA
-DEG",R46;ENT "H
IGH THETA-DEG",R
47⊢
2:
SCL R46,R4,-45,
5⊢
3:
CFG 1;0→R32;ENT
"ENT 9 FOR SECPA
T",R32;IF R32=9;
SFG 1;PRT "SEC P
AT"⊢
4:
ENT "COS TP-VOLT
AGE P30",R30;
PRT "COS TP VOLT
S ",R30⊢
5:
ENT "SPACING R31
",R31;PRT "SPACI
NG ",R31⊢
6:
ENT "NUM. ELEM.
R33",R33;PRT "NU
M. ELEM.",R33⊢
7:
ENT "AMP. VALUES
 R(A)";PRT "AMP.
 VALUES"⊢
8:
1→A⊢
9:
"K";ENT RA;RA→R(
R33+1-A)⊢
10:
IF R33/2>A;1+A→A
;GTO "K"⊢
11:
1→A⊢
12:
"L";PRT A,RA;
PRT "------"⊢
13:
IF R33>A;1+A→A;
GTO "L"⊢
14:
0→R34;1→A⊢
15:
"M";RA+R34→R34⊢
16:
IF R33>A;1+A→A;
GTO "M"⊢
17:
PRT "R34",R34⊢
18:
ENT "NU. OF BEAM
S",R35",R35⊢
19:
36→B⊢
20:
DSP "BEAM POS.NE
XT";STP ⊢
21:
"Q";ENT A[B]⊢
22:
PRT "BEAM",B;
PRT "------"⊢
23:
IF R35+.5>B;1+B→
B;GTO "Q"⊢
24:
0→R40;ENT "ANG D
ELTA DEG",R40⊢
25:
R46→Z⊢
26:
0→R39⊢
27:
"N";0→R41→R42→R4
3⊢
28:
0→A;36→B⊢
29:
"P";A+1→A⊢
30:
SIN RB→X⊢
31:
360*R31(A-R33/2-
.5)(SIN Z-X)→R44
⊢
32:
RACOS R44+R41→R4
1⊢
33:
RASIN R44+R42→R4
2⊢
34:
IF R33>A;GTO "P"
⊢
35:
IF R35+.5>B;1+B→
B;0→A;GTO "Q"⊢
```

HP-9820 PROGRAM FOR θ_{rms} EXACT
(use for any S/N ratio)
Appendix 3.3

```
36:
COS Z↑R30/R34÷
ABS √(R41↑2+R42↑
2)÷R43⊢
37:
R43/√R35÷R45⊢
38:
IF R32=9;R45÷R(5
1+R39)⊢
39:
IF R32=9;R45÷R(1
01+R39)⊢
40:
PLT Z,20LOG R45⊢
41:
IF R47>Z;R40+Z÷Z
;1+R39÷R39;GTO "
N"⊢
42:
IF FLG 1;GTO 44⊢
43:
PEN ;GTO 3⊢
44:
PEN ;SCL R46,R47
,0,1⊢
45:
R46÷Z;0÷R39⊢
46:
"R";R(101+R39)/R
(51+R39)÷R(151+R
39)⊢
47:
IF R(151+R39)>1;
1/R(151+R39)÷R(1
51+R39)⊢
48:
PLT Z,R(151+R39)
⊢
49:
IF R47>Z;R40+Z÷Z
;1+R39÷R39;GTO "
R"⊢
50:
PEN ;R46÷Z;0÷R39
⊢
51:
SCL R46,R47,-1,1
⊢
52:
"S";PLT Z+.5R40,
R(152+R39)-R(15
1+R39))/R40⊢
53:
IF R47>Z÷R40;R40
+Z÷Z;1+R39÷R39;
GTO "S"⊢
54:
ENT "S/N-DB",Y;R
46÷Z;0÷R39;PEN ;
SCL R46,R47,-5,5
;ENT "NU P",248⊢
55:
"V";(Y+20LOG (R
(51+R39)+R(52+R3
9))-LOG 2))/10÷R
49;1/10↑R49÷R49⊢
56:
(Y+20(LOG (R(101
+R39)+R(102+R39)
)-LOG 2))/10÷R50
;1/10↑R50÷R50⊢
57:
R40/(R(152+R39)-
R(151+R39))÷R0⊢
58:
(20/R40)LOG (R(1
51+R39)/R(152+R3
9))÷B;ABS B÷S⊢
59:
IF R49<.25;IF R5
0<.25;PLT Z+.5R4
0,(8.686/B)√((R4
9+R50)/2R48)⊢
60:
IF R50≤4;IF R50>
.25;PLT Z+.5R40,
ABS R0√(R49(.5/R
48+R50/16))⊢
61:
IF R50>4;PLT Z+.
5R40,ABS R0√(R49
(.5/R48+.78))⊢
62:
IF R47>Z+R40;R40
+Z÷Z;1+R39÷R39;
GTO "V"⊢
63:
END ⊢
R194
```